

A low Mach two-speed relaxation scheme for the compressible Euler equations with gravity

Claudius Birke^{*†}, Christophe Chalons[‡],
Christian Klingenberg^{*}

December 7, 2021

Abstract

We present a numerical approximation of the solutions of the Euler equations with a gravitational source term. On the basis of a Suliciu type relaxation model with two relaxation speeds, we construct an approximate Riemann solver, which is used in a first order Godunov-type finite volume scheme. This scheme can preserve both stationary solutions and the low Mach limit to the corresponding incompressible equations. In addition, we prove that our scheme preserves the positivity of density and internal energy, that it is entropy satisfying and also guarantees not to give rise to numerical checkerboard modes in the incompressible limit. Later we give an extension to second order that preserves these properties. Finally, the theoretical properties are investigated in numerical experiments.

Keywords Euler equations, finite volume methods, relaxation, well-balancing, low Mach, asymptotic-preserving, entropy satisfying, checkerboard modes, positivity preserving

AMS subject classification 35L65, 65M08, 76M12

1 Introduction

The goal of this paper is to find a numerical approximation of the solutions of the Euler equations including a gravitational source term. In a dimensionless form these equations are defined by

$$\begin{aligned} \partial_t \rho + \nabla \cdot (\rho \mathbf{u}) &= 0, \\ \partial_t (\rho \mathbf{u}) + \nabla \cdot (\rho \mathbf{u} \otimes \mathbf{u}) + \frac{1}{M^2} \nabla p &= -\frac{1}{M^2} \rho \nabla \Phi, \\ \partial_t E + \nabla \cdot ((E + p) \mathbf{u}) &= -\rho \mathbf{u} \cdot \nabla \Phi, \end{aligned} \tag{1.1}$$

^{*}Fakultät für Mathematik und Informatik, Universität Würzburg, Emil-Fischer-Str. 40, 97074 Würzburg, Germany

[†]Correspondence to: Claudius Birke, Universität Würzburg, Emil-Fischer-Str. 40, 97074 Würzburg, Germany, Email: claudius.birke@mathematik.uni-wuerzburg.de

[‡]Laboratoire de Mathématiques de Versailles, UVSQ, CNRS, Université Paris-Saclay, 78035 Versailles, France

where $\rho(x, t) > 0$ denotes the density, $\mathbf{u} \in \mathbb{R}^d$ the velocity vector, $E(x, t) > 0$ the total energy and $\Phi : \mathbb{R}^d \rightarrow \mathbb{R}$ a given smooth gravitational potential. In this dimensionless formulation, the parameter M represents the Mach number, which controls the ratio between the velocity of the gas and the speed of sound. The pressure is given by a pressure law $p(\tau, e) : \mathbb{R}^+ \times \mathbb{R}^+ \rightarrow \mathbb{R}^+$, where $\tau = 1/\rho$ denotes the specific volume and $e > 0$ the internal energy. The total energy can then be expressed by

$$E = \rho e + \frac{1}{2} M^2 \rho |\mathbf{u}|^2. \quad (1.2)$$

The pressure law closing this model obeys the second law of thermodynamics so that a specific entropy $s(\tau, e) : \mathbb{R}^+ \times \mathbb{R}^+ \rightarrow \mathbb{R}^+$, which satisfies the relation

$$-T ds = de + pd\tau \quad (1.3)$$

for some temperature $T(\tau, e) > 0$, exists. The phase space to which the system (1.1) is associated is denoted by

$$\Omega = \{(\rho, \rho \mathbf{u}, E) \in \mathbb{R}^{d+2}; \rho > 0, e > 0\}. \quad (1.4)$$

This model can be used in various fields of application, such as the simulation of gas flows in the interior of stars in astrophysics. Depending on the application, the flows can have large scale differences, e.g. the sound speed can be much higher than the speed of the fluid flow. In these low Mach number regimes standard finite volume schemes suffer from excessive diffusion, which can erase the structure of the solution beyond recognition. A number of different strategies have been developed to overcome this problem. One simple but efficient strategy is to modify the diffusion term in the numerical flux by rescaling it with the local Mach number and thereby reduce the viscosity on the velocity. First introduced for the homogeneous Euler equations [24, 1, 23, 10, 15, 25, 26, 32], this approach was also extended to the Euler equations including a gravitational source term [2]. A second approach introduced by Klein [22] relies on a pressure splitting, which decomposes the system of equations into one slow, non-linear part and into a linear part for the fast acoustic dynamics. The non-linear part can be solved explicitly by a shock-capturing method, while the linear part is to be solved implicitly due to its stiffness. Thomann *et al.* combine the idea of splitting the pressure with a Suliciu type relaxation approach [31]. The non-linear part is solved explicitly by a Godunov-type method based on an approximate Riemann solver, whereas the linear part is treated implicitly. Later this implicit-explicit (IMEX) approach was extended to the Euler equations with gravity [30].

Basis of the herein presented scheme is a third alternative introduced by Chalons *et al.* in [8], where a two-speed relaxation scheme for the barotropic, homogeneous Euler equations is proposed. The use of two different relaxation speeds enables an independent control of the numerical viscosity on the density and on the velocity. By special definitions of the speeds in the low Mach regime, viscosity is transferred from the velocity to the density. Therefore, this approach is related to the previously described rescaling of the viscosity term. The key advantage of this method is that under a subcharacteristic condition it is stable and provably entropy satisfying. Later the two-speed relaxation system was used to develop an IMEX scheme for the homogeneous Euler equations [9].

In contrast, the method presented in this paper is fully explicit. The basic structure of the two-speed relaxation system is adopted and extended by gravitational source terms. From the exact resolution of the Riemann problem associated with this relaxation system, a Godunov-type

finite volume method is constructed. The modification of the relaxation speeds is adopted from the original approach. The resulting approximate Riemann solver satisfies a discrete entropy inequality. Based on this inequality, it is shown that no checkerboard modes can arise in the variables fluid velocity and pressure. Checkerboard modes pose an instability characterized by a decoupling of the spatial approximation, which can occur in numerical solutions of incompressible fluid equations computed on collocated grids [17]. It is well-known that most of the asymptotic-preserving schemes exhibit such nonphysical checkerboard modes in low Mach regimes [14, 26]. When studying the Euler equations with gravity source terms one has to consider their influence on the behaviour of steady states. In several applications such as astrophysics one deals with problems close to the hydrostatic equilibrium

$$\begin{cases} \mathbf{u} = 0, \\ \nabla p = -\rho \nabla \Phi. \end{cases} \quad (1.5)$$

Standard finite volume schemes do not automatically satisfy a discrete equivalent of (1.5). Therefore these steady states are not preserved exactly by such schemes and small perturbations around this equilibrium cannot be resolved unless the resolution of the scheme is increased, so that the truncation error is sufficiently small. In order to avoid this potentially high computational effort, well-balanced schemes [12, 11, 30, 4, 3, 33, 21, 29, 20] were introduced, which satisfy exactly a discrete equivalent of the steady state.

The well-balancing mechanism in the herein presented relaxation scheme is taken over from [16]. The key idea is to add a transport relaxation equation for the gravitational potential to the relaxation system, which leads to a Riemann-problem that is under-determined. This gives an additional degree of freedom and allows to introduce a closure equation that is a discrete equivalent of (1.5) and ensures the well-balanced property. This approach is exact for certain families of hydrostatic equilibria, i.e. isothermal, incompressible and polytropic ones. In all other cases it maintains the equilibrium to second order. We extend this approach so that it can be applied to any hydrostatic solution for the Euler equations with any equation of state if the hydrostatic solution is known a priori. The extension is based on a second order approximation of the difference in the gravitational potential using the given hydrostatic states for the density and pressure. This is useful for applications in stellar astrophysics, in which the equation of state (EoS) is given in form of a table. Since hydrostatic solutions depend on the EoS, they can then only be found through numerical simulations carried out beforehand and are therefore available in the form of discrete data.

The paper is organized as follows. In section 2, the two-speed relaxation model is derived. In addition, the approximate Riemann solver associated with this system and its intermediate states are determined. The following section 3 contains the first order Godunov-type finite volume scheme, which is based on the previously introduced approximate Riemann solver. Its properties are described and proven in section 4. A suitable extension to second order in space is given in chapter 5. In chapter 6, the properties of the second order scheme are checked in numerical tests. Finally, chapter 7 provides the conclusion and an outlook.

2 The relaxation model

The relaxation system described below is based at its core on the Suliciu relaxation model [28, 7, 13]. The pressure p is approximated by the relaxation variable π and we add an additional

equation describing its behaviour to the system

$$\partial_t \rho \pi + \partial_x (\rho \pi v) + ab \partial_x v = \rho \frac{p - \pi}{\varepsilon}. \quad (2.1)$$

While only one relaxation speed is used in the classical Suliciu relaxation model, here two speeds $a > 0$ and $b > 0$ appear, as proposed in [8]. This will be useful to control viscosity for pressure and velocity separately. These speeds will be defined later in chapter 4.4 so that they meet stability criteria and keep the viscosity bounded in the low Mach regime.

In addition, also the velocity u is approximated by a relaxation variable v and the following equation is introduced

$$\partial_t (\rho v) + \partial_x (\rho v^2) + \frac{a}{b} \partial_x \frac{\pi}{M^2} = \rho \frac{u - v}{\varepsilon} - \frac{a}{b} \frac{1}{M^2} \rho \partial_x \Phi. \quad (2.2)$$

In the next step, we also want to include the gravitational potential in the approximate Riemann solver. According to [16] this can be done by approximating the gravitational potential Φ by the relaxation variable Z and adding a transport relaxation equation to the relaxation system

$$\partial_t \rho Z + \partial_x \rho v Z = \rho \frac{\Phi - Z}{\varepsilon}. \quad (2.3)$$

Finally, we derive the following relaxation model

$$\begin{aligned} \partial_t \rho + \partial_x (\rho v) &= 0, \\ \partial_t (\rho u) + \partial_x \left(\rho u v + \frac{\pi}{M^2} \right) &= -\frac{1}{M^2} \rho \partial_x Z, \\ \partial_t E + \partial_x ((E + \pi) v) &= -\rho v \partial_x Z, \\ \partial_t (\rho \pi) + \partial_x (\rho \pi v) + ab \partial_x v &= \rho \frac{p - \pi}{\varepsilon}, \\ \partial_t (\rho v) + \partial_x (\rho v^2) + \frac{a}{b} \partial_x \frac{\pi}{M^2} &= \rho \frac{u - v}{\varepsilon} - \frac{a}{b} \frac{1}{M^2} \rho \partial_x Z, \\ \partial_t \rho Z + \partial_x \rho v Z &= \rho \frac{\Phi - Z}{\varepsilon}, \\ \partial_t a + v \partial_x a &= 0, \\ \partial_t b + v \partial_x b &= 0. \end{aligned} \quad (2.4)$$

The solutions to this relaxation model can be seen as a viscous approximation of the solutions of the original system (1.1) as long as the subcharacteristic conditions

$$a \geq b \quad \text{and} \quad ab \geq \rho^2 c^2 \quad (2.5)$$

are satisfied.

Remark 1 *By choosing $u = v$ and $a = b$ one recovers the standard Suliciu relaxation model.*

The homogeneous system, denoted by $(2.4)_{\varepsilon=\infty}$, has the following properties.

Lemma 1 *The relaxation system $(2.4)_{\varepsilon=\infty}$ is hyperbolic and all characteristic fields are linearly degenerate. The eigenvalues of the system are given by*

$$\sigma^v = v, \quad \sigma^\pm = v \pm \frac{a}{M\rho} \quad (2.6)$$

where λ^v has multiplicity six. The eigenvalues have the fixed ordering

$$\sigma^- < \sigma^v < \sigma^+. \quad (2.7)$$

The Riemann invariant corresponding to the eigenvalue σ^v is

$$I_1^v = v \quad (2.8)$$

and those corresponding to σ^\pm are

$$\begin{aligned} I_1^\pm &= v \pm \frac{a}{M\rho}, \quad I_2^\pm = u \pm \frac{b}{M\rho}, \quad I_3^\pm = \frac{1}{\rho} + \frac{\pi}{ab}, \\ I_4^\pm &= e + \frac{(a-b)b + 2\rho(\pi \pm bM(v-u))}{2\rho^2}, \\ I_5^\pm &= a, \quad I_6^\pm = b, \quad I_7^\pm = Z. \end{aligned} \quad (2.9)$$

Proof. The computations are straightforward and left to the reader. \square

Remark 2 The relaxation system $(2.4)_{\varepsilon=\infty}$ provides only one Riemann invariant I_1^v for the contact wave. As a result, the associated Riemann problem is under-determined.

Let us now consider a single Riemann problem associated with the system $(2.4)_{\varepsilon=\infty}$. In order to simplify the notations we introduce the vector of conservative variables

$$W = (\rho, \rho u, E, \rho\pi, \rho v, \rho Z, a, b). \quad (2.10)$$

Then the initial data of the Riemann problem is given by two constant states W^L and W^R separated by one discontinuity located at $x = 0$

$$W_0(x) = \begin{cases} W^L, & x < 0, \\ W^R, & x > 0. \end{cases} \quad (2.11)$$

The solution to this problem consists of four constant states, each separated by a contact discontinuity. Therefore the approximate Riemann solver $W_{\mathcal{R}}(x/t; W^L, W^R)$ has the structure

$$W_{\mathcal{R}}\left(\frac{x}{t}, W^L, W^R\right) = \begin{cases} W^L, & \frac{x}{t} < \sigma^-, \\ W^{L*}, & \sigma^- < \frac{x}{t} < \sigma^v, \\ W^{R*}, & \sigma^v < \frac{x}{t} < \sigma^+, \\ W^R, & \sigma^+ < \frac{x}{t}. \end{cases} \quad (2.12)$$

This structure of the solution is also shown in Fig. 1. For the computation of the intermediate states W^{L*} and W^{R*} we can use the Riemann invariants given in lemma 1. Since Riemann invariants are constant across their corresponding wave, each Riemann invariant provides one equation. However, counting the Riemann invariants reveals that only 15 Riemann invariants face 16 unknown intermediate states. Therefore, the Riemann problem (2.11) is, as already stated in remark 2, under-determined. In order to overcome this problem, it is suggested in [16] to introduce an additional relation

$$\pi^{R*} - \pi^{L*} = -\bar{\rho}(W^L, W^R)(Z^R - Z^L), \quad (2.13)$$

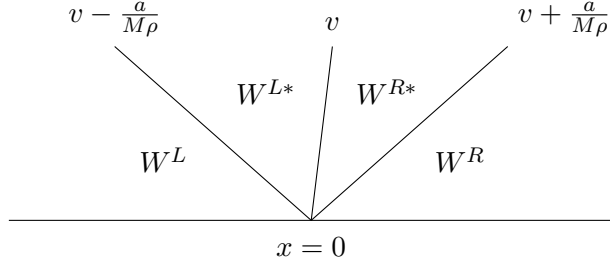


Fig. 1 Schematic diagram of the Riemann fan for the relaxation system (2.4). The Riemann fan consists of the two intermediate states W^{L*} and W^{R*} for given states W^L and W^R . The states are separated by the three wave speeds $v - a/(M\rho)$, v and $v + a/(M\rho)$

where the function $\bar{\rho}$ denotes a ρ -average function. This equation is chosen because it is a discrete representation of the steady states at rest in (1.5) in one spatial dimension and therefore will be useful for the well-balancing of hydrostatic equilibria. The explicit definition of the function $\bar{\rho}$ depends on the underlying hydrostatic equilibrium and will be given later in chapter 4.5.

With the newly added closure equation, it is now possible to compute the intermediate states in the Riemann solution.

Lemma 2 *The solution of the Riemann problem (2.11) associated with the relaxation system (2.4) $_{\varepsilon=\infty}$ has the structure given in (2.12) with the intermediate states*

$$v^* = \frac{Mb^L v^L + Mb^R v^R + \pi^L - \pi^R - \bar{\rho}(W^L, W^R)(Z^R - Z^L)}{M(b^L + b^R)}, \quad (2.14)$$

$$\frac{1}{\rho^{L*}} = \frac{1}{\rho^L} + \frac{Mb^R(v^R - v^L) + \pi^L - \pi^R - \bar{\rho}(W^L, W^R)(Z^R - Z^L)}{a^L(b^L + b^R)}, \quad (2.15)$$

$$\frac{1}{\rho^{R*}} = \frac{1}{\rho^R} + \frac{Mb^L(v^R - v^L) + \pi^R - \pi^L + \bar{\rho}(W^L, W^R)(Z^R - Z^L)}{a^R(b^L + b^R)}, \quad (2.16)$$

$$u^{L*} = u^L + \frac{b^L}{Ma^L(b^L + b^R)}(b^R M(v^R - v^L) + \pi^L - \pi^R - \bar{\rho}(W^L, W^R)(Z^R - Z^L)), \quad (2.17)$$

$$u^{R*} = u^R + \frac{b^R}{Ma^R(b^L + b^R)}(b^L M(v^L - v^R) + \pi^L - \pi^R - \bar{\rho}(W^L, W^R)(Z^R - Z^L)), \quad (2.18)$$

$$\pi^{L*} = \frac{b^R \pi^L + b^L \pi^R + Mb^L b^R(v^L - v^R) + b^L \bar{\rho}(W^L, W^R)(Z^R - Z^L)}{b^L + b^R}, \quad (2.19)$$

$$\pi^{R*} = \frac{b^R \pi^L + b^L \pi^R + Mb^L b^R(v^L - v^R) - b^R \bar{\rho}(W^L, W^R)(Z^R - Z^L)}{b^L + b^R}, \quad (2.20)$$

$$e^{L*} = e^L + \frac{(\pi^{L*})^2 - (\pi^L)^2}{2a^L b^L} + \frac{(v^* - u^{L*})^2 - (v^L - u^L)^2}{2(\frac{a^L}{b^L} - 1)}, \quad (2.21)$$

$$e^{R*} = e^R + \frac{(\pi^{R*})^2 - (\pi^R)^2}{2a^R b^R} + \frac{(v^* - u^{R*})^2 - (v^R - u^R)^2}{2(\frac{a^R}{b^R} - 1)}, \quad (2.22)$$

$$a^{L*} = a^L, \quad a^{R*} = a^R, \quad b^{L*} = b^L, \quad b^{R*} = b^R, \quad Z^{L*} = Z^L, \quad Z^{R*} = Z^R. \quad (2.23)$$

Proof. The intermediate states can be computed by solving the system of equations given by the Riemann invariants and the closure equation (2.13). The precise steps are straightforward and therefore left to the reader. \square

Remark 3 *At this point, we do not explicitly define the relaxation speeds a^L , a^R , b^L and b^R , since later, in the proofs of the properties of the relaxation method, various conditions are placed on these speeds. The explicit definitions are then provided in chapter 4.4.*

Equipped with the approximate Riemann solver, we can now define the overall discretization of the scheme in the next chapter.

3 The relaxation scheme

Before we derive a complete finite volume scheme for the Euler equations with a gravitational source (1.1), we introduce some useful notations. The spatial domain is divided into cells $\mathcal{C}_i = (x_{i-1/2}, x_{i+1/2})$ with $i \in \mathbb{Z}$ that have the size $\Delta x = x_{i+1/2} - x_{i-1/2}$. The cell centers are denoted by x_i . The time discretization is given by $t^n = n\Delta t$ with $n \in \mathbb{N}$ and a timestep Δt that is restricted by the CFL condition

$$\frac{\Delta t}{\Delta x} \max_i \left\{ \left| v_i - \frac{a_i}{M\rho_i} \right|, \left| v_i + \frac{a_i}{M\rho_i} \right| \right\} \leq \frac{1}{2}. \quad (3.1)$$

The cell average W_i^n then approximates the value over the cell \mathcal{C}_i at time t^n

$$W_i^n \approx \frac{1}{\Delta x} \int_{\mathcal{C}_i} W(x, t^n) dx. \quad (3.2)$$

Using the solutions to the local Riemann problems obtained by the approximate Riemann solver $W_{\mathcal{R}}$ (2.12), the cell averages can be updated to the time level t^{n+1} by a Godunov method of the form

$$\begin{aligned} W_i^{n+1} = & W_i^n - \frac{\Delta t}{\Delta x} \left(F_{i+1/2}^n - F_{i-1/2}^n \right) \\ & + \frac{\Delta t}{2} \left(s^+(W_{i-1}^n, W_i^n) \frac{\Phi_i^n - \Phi_{i-1}^n}{\Delta x} + s^-(W_i^n, W_{i+1}^n) \frac{\Phi_{i+1}^n - \Phi_i^n}{\Delta x} \right), \quad (3.3) \\ F_{i+1/2}^n = & F(W_i^n, W_{i+1}^n). \end{aligned}$$

The numerical flux is defined by

$$F(W^L, W^R) = \begin{cases} F(W^L), & \text{if } \sigma^- > 0, \\ F^{L*}, & \text{if } \sigma^- < 0 \leq \sigma^v, \\ F^{R*}, & \text{if } \sigma^v < 0 < \sigma^+, \\ F(W^R), & \text{if } \sigma^+ < 0, \end{cases} \quad (3.4)$$

where according to the left-hand sides of the first three equations of (2.4) the intermediate fluxes can be written as

$$\begin{aligned} F^{L*} = & \left(\rho^{L*} v^*, \rho^{L*} u^{L*} v^* + \frac{\pi^{L*}}{M^2}, (E^{L*} + \pi^{L*}) v^* \right), \\ F^{R*} = & \left(\rho^{R*} v^*, \rho^{R*} u^{R*} v^* + \frac{\pi^{R*}}{M^2}, (E^{R*} + \pi^{R*}) v^* \right). \end{aligned} \quad (3.5)$$

The numerical source terms are set as follows

$$\begin{aligned} s^+(W^L, W^R) = & -(\text{sgn}(v^*) + 1) \left(0, \frac{1}{M^2} \bar{\rho}(W^L, W^R), \bar{\rho}(W^L, W^R) v^* \right)^T, \\ s^-(W^L, W^R) = & (\text{sgn}(v^*) - 1) \left(0, \frac{1}{M^2} \bar{\rho}(W^L, W^R), \bar{\rho}(W^L, W^R) v^* \right)^T. \end{aligned} \quad (3.6)$$

4 Properties of the relaxation scheme

In this chapter we focus on the properties of the relaxation scheme just described. We start with the property of entropy stability.

4.1 Entropy inequality

In general, finite volume methods do not automatically reflect the physical behaviour of a fluid correctly, as they are based on the concept of weak formulations and consequently search for weak solutions. Unfortunately, these weak solutions are not unique. It therefore makes sense that solutions produced by the scheme do satisfy additional conditions so that physically incorrect solutions are ruled out.

Going back to the Euler equations (1.1) and assuming smooth solutions, it is possible to derive the additional conservation law

$$\partial_t \rho \mathcal{F}(s) + \partial_x \rho \mathcal{F}(s) u = 0 \quad (4.1)$$

for all smooth functions \mathcal{F} . This equation states that the entropy is conserved for smooth solutions. However, since the Euler equations are non-linear, discontinuities can arise in the solution in finite time despite of smooth initial conditions. At discontinuities the equation (4.1) is not valid, since it does not consider the entropy dissipation at shocks. According to the second law of thermodynamics the entropy can physically only increase. Mathematically, on the other hand, it is desirable to constrain the solution by initial and boundary conditions and therefore the sign of the entropy is reversed so that it can only decrease in time. Therefore, we replace the equality in (4.1) by an inequality, which leads to the following entropy inequality

$$\partial_t \rho \mathcal{F}(s) + \partial_x \rho \mathcal{F}(s) u \leq 0. \quad (4.2)$$

Our scheme should now mimic this behaviour in the sense that its solutions satisfy a discrete version of (4.2). The main effort is to show that the approximate Riemann solver associated with the scheme is consistent with the entropy inequality in the sense of Harten, Lax and van Leer [18]. This property is stated in the following theorem.

Theorem 1 *Let W^L and W^R be two states of Ω . The values $a^{L,R}$ and $b^{L,R}$ are such that they satisfy the subcharacteristic Whitham conditions*

$$a^L b^L > p(\tau^L, e^L) \partial_e p(\tau^L, e^L) - \partial_\tau p(\tau^L, e^L), \quad (4.3)$$

$$a^L b^L > p(\tau^{L*}, e^{L*}) \partial_e p(\tau^{L*}, e^{L*}) - \partial_\tau p(\tau^{L*}, e^{L*}), \quad (4.4)$$

$$a^R b^R > p(\tau^{R*}, e^{R*}) \partial_e p(\tau^{R*}, e^{R*}) - \partial_\tau p(\tau^{R*}, e^{R*}), \quad (4.5)$$

$$a^R b^R > p(\tau^R, e^R) \partial_e p(\tau^R, e^R) - \partial_\tau p(\tau^R, e^R). \quad (4.6)$$

Furthermore, the following CFL restriction shall be satisfied

$$\frac{\Delta t}{\Delta x} \max \left\{ \left| v^L - \frac{a^L}{\rho^L} \right|, \left| v^R + \frac{a^R}{\rho^R} \right| \right\} \leq \frac{1}{2}. \quad (4.7)$$

Then the approximate Riemann solver $W_{\mathcal{R}}$ satisfies the inequality

$$\begin{aligned} \frac{1}{\Delta x} \int_{-\Delta x/2}^{\Delta x/2} (\rho \mathcal{F}(s)) \left(W_{\mathcal{R}} \left(\frac{x}{\Delta t}; W^L, W^R \right) \right) dx \leq \\ \frac{1}{2} (\rho^L \mathcal{F}(s^L) + \rho^R \mathcal{F}(s^R)) - \frac{\Delta t}{\Delta x} (\rho^R \mathcal{F}(s^R) v^R - \rho^L \mathcal{F}(s^L) v^L). \end{aligned} \quad (4.8)$$

Proof. The proof of this theorem follows the same steps as the proof in [16, p. 12], only the definition of the second Riemann invariant J changes to

$$J(W) := J(\pi, \hat{e}) = \hat{e} - \frac{\pi^2}{2ab} \quad \text{with } \hat{e} = e - \frac{(v-u)^2}{2(\frac{a}{b}-1)}. \quad (4.9)$$

This difference is due to the attachment of the additional velocity equation (2.2) to the relaxation system. \square

Remark 4 *An important step in establishing the entropy inequality is to show that the specific relaxation entropy is greater than or equal to the specific entropy of the original system, i.e.*

$$\hat{s} \geq s. \quad (4.10)$$

Since the function $\rho\mathcal{F}$ is convex, the direct consequence of (4.10) is that the relaxation entropy is greater than or equal to the entropy

$$\rho\mathcal{F}(\hat{s}) \geq \rho\mathcal{F}(s). \quad (4.11)$$

Equality in both inequalities is only reached in the equilibrium.

4.2 Prevention of checkerboard modes

It has already been pointed out in the introduction that for asymptotic preserving schemes checkerboards can arise in the low Mach regime. Of course, it is desirable to prevent the occurrence of such an unphysical phenomenon.

Theorem 2 *The relaxation scheme prevents the occurrence of checkerboard modes in the velocity and pressure variables.*

Proof. The proof builds on the entropy inequality of the previous chapter and follows the strategy of a similar proof in [8]. In order to simplify the notation we denote the entropy by $\eta = \rho\mathcal{F}(s)$ and the entropy flux by $G = \rho\mathcal{F}(s)u$. Analogously, the relaxation entropy is denoted by $\Sigma = \rho\mathcal{F}(\hat{s})$ and the relaxation entropy flux by $G^r = \rho\mathcal{F}(\hat{s})u$. Furthermore, we rewrite the entropy inequality (4.8) in the equivalent form

$$\eta(W_i^{n+1}) - \eta(W_i^n) + \frac{\Delta t}{\Delta x} (G_{i+1/2}^n - G_{i-1/2}^n) \leq 0. \quad (4.12)$$

This inequality can be rewritten by

$$\eta(W_i^{n+1}) \leq \eta(W_i^n) - \frac{\Delta t}{\Delta x} (G_{i+1/2}^n - G_{i-1/2}^n) = \frac{1}{\Delta x} \int_{x_{i-1/2}}^{x_{i+1/2}} \Sigma(W_{\mathcal{R}}(t^{n+1}, x)) dx. \quad (4.13)$$

Additionally, by using Jensen's inequality and (4.11) we can state the following inequalities

$$\eta(W_i^{n+1}) \leq \frac{1}{\Delta x} \int_{x_{i-1/2}}^{x_{i+1/2}} \eta(W(t^{n+1}, x)) dx \leq \frac{1}{\Delta x} \int_{x_{i-1/2}}^{x_{i+1/2}} \Sigma(W_{\mathcal{R}}(t^{n+1}, x)) dx. \quad (4.14)$$

We now define the left-hand side of the inequality (4.12) by

$$D_i^n := \eta(W_i^{n+1}) - \eta(W_i^n) + \frac{\Delta t}{\Delta x} (G_{i+1/2}^n - G_{i-1/2}^n). \quad (4.15)$$

For steady and space periodic solutions we then have

$$\sum_i D_i^n = 0. \quad (4.16)$$

In combination with the entropy inequality (4.12) we get

$$D_i^n = 0 \quad \forall i. \quad (4.17)$$

From this follows directly that all the inequalities in (4.14) are replaced by equalities and therefore the entropy is equal to the relaxation entropy,

$$\eta(W(t^{n+1}, x)) = \Sigma(W_{\mathcal{R}}(t^{n+1}, x)). \quad (4.18)$$

In the proof of the entropy inequality it is shown that this is just the case in the equilibrium, so only if

$$\pi = p(\rho, e), \quad u = v, \quad \tau = \frac{1}{\rho}, \quad \hat{s} = s. \quad (4.19)$$

As a consequence, the following relations apply to a single Riemann problem

$$\begin{aligned} \tau^{L*} &= \frac{1}{\rho^{L*}}, \quad \tau^{R*} = \frac{1}{\rho^{R*}}, \quad v^* = u^{L*} = u^{R*}, \\ \pi^{L*} &= p(\rho^{L*}, e^{L*}) = p(\rho^{L*}, s^{L*}), \quad \pi^{R*} = p(\rho^{R*}, e^{R*}) = p(\rho^{R*}, s^{R*}). \end{aligned} \quad (4.20)$$

Since τ is a Riemann invariant for σ^- and σ^+ , it holds

$$\tau^{L*} = \tau^L, \quad \tau^{R*} = \tau^R. \quad (4.21)$$

We can use this fact to gain more information about the intermediate densities

$$\begin{aligned} \frac{1}{\rho^{L*}} = \tau^{L*} = \frac{1}{\rho^L} &\Rightarrow \rho^{L*} = \rho^L, \\ \frac{1}{\rho^{R*}} = \tau^{R*} = \frac{1}{\rho^R} &\Rightarrow \rho^{R*} = \rho^R. \end{aligned} \quad (4.22)$$

From the explicit definition of the intermediate states in (2.15) and (2.16) we can deduce that

$$\frac{1}{\rho^{L*}} - \frac{1}{\rho^L} = \frac{Mb^R (v^R - v^L) + \pi^L - \pi^R - \bar{\rho} (W^L, W^R) (Z^R - Z^L)}{a^L (b^L + b^R)} = 0, \quad (4.23)$$

$$\frac{1}{\rho^{R*}} - \frac{1}{\rho^R} = \frac{Mb^L (v^R - v^L) + \pi^R - \pi^L + \bar{\rho} (W^L, W^R) (Z^R - Z^L)}{a^R (b^L + b^R)} = 0. \quad (4.24)$$

With a look at the intermediate states u^{L*} and u^{R*} , we see that we can use (4.23) and (4.24) to get

$$u^{L*} = u^L + \frac{b^L}{M} \frac{Mb^R (v^R - v^L) + \pi^L - \pi^R - \bar{\rho} (W^L, W^R) (Z^R - Z^L)}{a^L (b^L + b^R)} = u^L, \quad (4.25)$$

$$u^{R*} = u^R + \frac{b^R}{M} \frac{Mb^L (v^L - v^R) + \pi^L - \pi^R + \bar{\rho} (W^L, W^R) (Z^R - Z^L)}{a^R (b^L + b^R)} = u^R. \quad (4.26)$$

Since we are at equilibrium we can conclude that

$$v^* = u^{L*} = u^{R*} = u^L = u^R = v^L = v^R. \quad (4.27)$$

In the next part we will show that the left and the right state at the interface are equal for π . From the Riemann invariants in (2.9) we take

$$I_4^\pm = \frac{1}{\rho} + \frac{\pi}{2ab}. \quad (4.28)$$

This quantity is constant across the left and right waves in the Riemann fan which means

$$\begin{aligned} \frac{1}{\rho^{L*}} + \frac{\pi^{L*}}{2a^L b^L} &= \frac{1}{\rho^L} + \frac{\pi^L}{2a^L b^L}, \\ \frac{1}{\rho^{R*}} + \frac{\pi^{R*}}{2a^R b^R} &= \frac{1}{\rho^R} + \frac{\pi^R}{2a^R b^R}. \end{aligned} \quad (4.29)$$

It has already been established in (4.22) that the density has only two states and therefore we can simplify the equations to

$$\begin{aligned} \pi^{L*} &= \pi^L \\ \pi^{R*} &= \pi^R. \end{aligned} \quad (4.30)$$

From the explicit definition of the intermediate states and the closure equation (2.13) follows

$$\begin{aligned} \pi^{L*} = \pi^L &= \frac{b^R \pi^L + b^L \pi^R + Mb^L b^R (v^L - v^R) - b^L \bar{\rho}(W^L, W^R) (Z^R - Z^L)}{b^L + b^R} \\ &\stackrel{(4.27)}{=} \frac{b^R \pi^L + b^L \pi^R - b^L \bar{\rho}(W^L, W^R) (Z^R - Z^L)}{b^L + b^R} \\ &\stackrel{(2.13)}{=} \frac{b^R \pi^L + b^L \pi^R + b^L (\pi^R - \pi^L)}{b^L + b^R}. \end{aligned} \quad (4.31)$$

Solving for π^L gives

$$\pi^L = \pi^R. \quad (4.32)$$

Thus we have shown that for both velocities and the pressure, the left and right states at the interface are equal. The solution in these quantities is therefore constant in space and checkerboards cannot occur. \square

Remark 5 *For pressure laws that depend only on density, it can also be proven that the density and the internal energy are constant for steady and space periodic solutions. Therefore, in this case, no checkerboard modes can occur in these quantities.*

4.3 Positivity preserving property

For the robustness of a scheme it is essential to keep especially the density but also the internal energy positive. The following lemma will guarantee this property.

Lemma 3 Given $W^L, W^R \in \Omega$. If the relaxation speeds a^L and a^R are large enough to ensure

$$v^L - \frac{a^L}{M\rho^L} < v^* < v^R + \frac{a^R}{M\rho^R}, \quad (4.33)$$

$$e^L + \frac{(\pi^{L*})^2 - (\pi^L)^2}{2a^L b^L} + \frac{(v^* - u^{L*})^2 - (v^L - u^L)^2}{2(\frac{a^L}{b^L} - 1)} > 0, \quad (4.34)$$

$$e^R + \frac{(\pi^{R*})^2 - (\pi^R)^2}{2a^R b^R} + \frac{(v^* - u^{R*})^2 - (v^R - u^R)^2}{2(\frac{a^R}{b^R} - 1)} > 0, \quad (4.35)$$

then the approximate Riemann solver $W_{\mathcal{R}}$ preserves the positivity of the density and internal energy.

Proof. First, it is trivial that the conditions (4.33), (4.34) and (4.35) are satisfied for a sufficiently large a . To prove the positivity of the density in a next step, we start with the Riemann invariants I_1^\pm from lemma 1, which give us

$$v^L - \frac{a^L}{M\rho^L} = v^* - \frac{a^L}{M\rho^{L*}} \quad \text{and} \quad v^R + \frac{a^R}{M\rho^R} = v^* + \frac{a^R}{M\rho^{R*}}. \quad (4.36)$$

Using these relations, we can rewrite (4.33) by

$$-\rho^{L*} < 0 < \rho^{R*}. \quad (4.37)$$

So, the intermediate states for the density are positive. The positivity of the internal energy directly follows from (4.34) and (4.35), since the left-hand sides of these conditions represent the left and right intermediate states of the internal energy. \square

Clearly, this lemma is of limited use in practice. It states that in principle it is possible to preserve the positivity, but it does not help to find a suitable definition of the relaxation speeds that works generally. The following lemma, which is inspired by [8], gives stricter conditions for the relaxation speeds, which can also be used for their explicit definition. Under these conditions, it can be proven that the density is kept positive.

Lemma 4 Consider the relaxation solver with intermediate values and speeds defined by (2.14)-(2.23) with the initial data at equilibrium. Assume that the relaxation speeds a^L , a^R , b^L , b^R satisfy

$$a^L \geq b^L, \quad a^R \geq b^R, \quad (4.38)$$

$$\frac{b^L}{\rho^L} \geq a_q^L, \quad \frac{b^R}{\rho^R} \geq a_q^R, \quad (4.39)$$

$$\frac{\sqrt{a^L b^L}}{\rho^L} \geq c^L (1 + \beta X^L), \quad \frac{\sqrt{a^R b^R}}{\rho^R} \geq c^R (1 + \beta X^R). \quad (4.40)$$

for some a_q^L and a_q^R depending on W^L , W^R and X^L , X^R defined by (4.43) and (4.44) with a positive parameter β . The quantities c^L, c^R represent the sound speed. Then the approximate Riemann solver $W_{\mathcal{R}}$ preserves the positivity of the density.

Proof. We start with the definition of the intermediate density (2.15)

$$\begin{aligned}
\frac{1}{\rho^{L*}} &= \frac{1}{\rho^L} + \frac{Mb^R(v^R - v^L) + \pi^L - \pi^R - \bar{\rho}(W^L, W^R)(Z^R - Z^L)}{a^L(b^L + b^R)} \\
&\geq \frac{1}{\rho^L} - \frac{Mb^R(v^L - v^R)_+}{a^L(b^L + b^R)} - \frac{(\pi^R - \pi^L)_+}{a^L(b^L + b^R)} - \frac{\bar{\rho}(W^L, W^R)(Z^R - Z^L)_+}{a^L(b^L + b^R)} \\
&\geq \frac{1}{\rho^L} - \frac{M(v^L - v^R)_+}{a^L} - \frac{(\pi^R - \pi^L)_+}{a^L(\rho^L a_q^L + \rho^R a_q^R)} - \frac{\bar{\rho}(W^L, W^R)(Z^R - Z^L)_+}{a^L(\rho^L a_q^L + \rho^R a_q^R)}. \tag{4.41}
\end{aligned}$$

Analogously, we get

$$\frac{1}{\rho^{R*}} \geq \frac{1}{\rho^R} - \frac{M(v^L - v^R)_+}{a^R} - \frac{(\pi^L - \pi^R)_+}{a^R(\rho^L a_q^L + \rho^R a_q^R)} - \frac{\bar{\rho}(W^L, W^R)(Z^L - Z^R)_+}{a^R(\rho^L a_q^L + \rho^R a_q^R)}. \tag{4.42}$$

Let us now define the variables

$$X^L = \frac{1}{c^L} \left[M(v^L - v^R)_+ + \frac{(\pi^R - \pi^L)_+}{\rho^L a_q^L + \rho^R a_q^R} + \frac{\bar{\rho}(W^L, W^R)(Z^R - Z^L)_+}{\rho^L a_q^L + \rho^R a_q^R} \right], \tag{4.43}$$

$$X^R = \frac{1}{c^R} \left[M(v^L - v^R)_+ + \frac{(\pi^L - \pi^R)_+}{\rho^L a_q^L + \rho^R a_q^R} + \frac{\bar{\rho}(W^L, W^R)(Z^L - Z^R)_+}{\rho^L a_q^L + \rho^R a_q^R} \right], \tag{4.44}$$

in order to rewrite the former inequalities in the form

$$\begin{aligned}
\frac{1}{\rho^{L*}} &\geq \frac{1}{\rho^L} \left(1 - \frac{\rho^L c^L}{a^L} X^L \right), \\
\frac{1}{\rho^{R*}} &\geq \frac{1}{\rho^R} \left(1 - \frac{\rho^R c^R}{a^R} X^R \right). \tag{4.45}
\end{aligned}$$

From combining the conditions (4.38) and (4.40), it follows that

$$\begin{aligned}
\frac{a^L}{\rho^L} \geq c^L(1 + \beta X^L) &\Rightarrow \frac{\rho^L c^L}{a^L} \leq \frac{1}{1 + \beta X^L}, \\
\frac{a^R}{\rho^R} \geq c^R(1 + \beta X^R) &\Rightarrow \frac{\rho^R c^R}{a^R} \leq \frac{1}{1 + \beta X^R}. \tag{4.46}
\end{aligned}$$

With these inequalities we rewrite (4.45)

$$\begin{aligned}
\frac{1}{\rho^{L*}} &\geq \frac{1}{\rho^L} \left(1 - \frac{X^L}{1 + \beta X^L} \right), \\
\frac{1}{\rho^{R*}} &\geq \frac{1}{\rho^R} \left(1 - \frac{X^R}{1 + \beta X^R} \right). \tag{4.47}
\end{aligned}$$

Because of the definitions in (4.43) and (4.44) we know that $X^L, X^R > 0$ and therefore we can conclude that

$$\rho^{L*} > 0, \quad \rho^{R*} > 0. \tag{4.48}$$

□

A similar proof for the positivity of the internal energy would be complicated due to the more complex structure of its intermediate states. Therefore, we choose a different way of proof, based on the proof of the entropy inequality in section 4.1.

Lemma 5 *Under the conditions of theorem 1 for the entropy inequality, the approximate Riemann solver $W_{\mathcal{R}}$ preserves the positivity of the internal energy.*

Proof. In remark 4 it is stated that the specific relaxation entropy is larger than the specific entropy of the original system. Therefore, we can conclude

$$s_i^{n+1} \geq s(\rho_i^{n+1}, e_i^{n+1}). \quad (4.49)$$

Furthermore, from relation (1.3) it follows that

$$\partial_s e(\tau, s) = -T(\tau, e) < 0. \quad (4.50)$$

By combining these two statements, it becomes clear that the updated internal energy remains positive

$$e_i^{n+1} \geq e(\rho_i^{n+1}, s_i^{n+1}) > 0. \quad (4.51)$$

□

4.4 Asymptotic preserving property

In the low Mach limit, the solutions of the Euler equations (1.1) tend to the solutions of the incompressible Euler equations. This behaviour can be illustrated by inserting expansions in terms of M given by

$$\begin{aligned} \rho &= \rho_0 + M\rho_1 + M^2\rho_2 + \mathcal{O}(M^3), & \mathbf{u} &= \mathbf{u}_0 + M\mathbf{u}_1 + M^2\mathbf{u}_2 + \mathcal{O}(M^3), \\ e &= e_0 + Me_1 + M^2e_2 + \mathcal{O}(M^3), & p &= p_0 + Mp_1 + M^2p_2 + \mathcal{O}(M^3), \end{aligned} \quad (4.52)$$

into the Euler equations (1.1). Now one can collect terms of order $\mathcal{O}(M^{-2})$

$$\nabla p_0 = -\rho_0 \nabla \Phi, \quad (4.53)$$

of order $\mathcal{O}(M^{-1})$

$$\nabla p_1 = -\rho_1 \nabla \Phi, \quad (4.54)$$

and finally of order $\mathcal{O}(1)$

$$\begin{aligned} \nabla \cdot (\rho_0 \mathbf{u}_0) &= 0, \\ \partial \mathbf{u}_0 + \mathbf{u}_0 \cdot \nabla \mathbf{u}_0 + \frac{\nabla p_2}{\rho_0} &= -\frac{\rho_2 \nabla \Phi}{\rho_0}, \\ \partial_t e_0 + \mathbf{u}_0 \cdot \nabla e_0 + \frac{1}{\rho_0} \nabla \cdot (p_0 \mathbf{u}_0) &= -\mathbf{u}_0 \cdot \nabla \Phi. \end{aligned} \quad (4.55)$$

These equations describe incompressible flows. The conditions (4.53) and (4.54) show that the couples ρ_0, p_0 and ρ_1, p_1 fulfil the hydrostatic equilibrium. For an ideal gas law the energy equation can be rewritten in the form

$$\nabla \cdot \mathbf{u}_0 = \frac{\mathbf{u}_0 \cdot \nabla \Phi}{c_0^2}. \quad (4.56)$$

The detailed derivation of this equation can be found in appendix A.

In the next step, we want to analyse to what extent the solutions of the compressible Euler equations correspond to those of the incompressible equations. Under the assumptions that in the density no constant fluctuations occur, i.e.

$$\rho = \rho_0 + \mathcal{O}(M^2), \quad (4.57)$$

and that the hydrostatic equilibrium is fulfilled up to errors of order $\mathcal{O}(M^2)$

$$\nabla p + \rho \nabla \Phi = \mathcal{O}(M^2), \quad (4.58)$$

the Euler equations (1.1) become

$$\begin{aligned} \nabla \cdot (\rho \mathbf{u}) &= \mathcal{O}(M^2), \\ \partial_t \mathbf{u} + \mathbf{u} \cdot \nabla \mathbf{u} + \frac{\nabla p_2}{\rho_0} &= -\frac{\rho_2 \nabla \Phi}{\rho_0} + \mathcal{O}(M^2), \\ \partial_t e + \mathbf{u} \cdot \nabla e + \frac{1}{\rho_0} \nabla \cdot (p \mathbf{u}) &= -\mathbf{u} \cdot \nabla \Phi + \mathcal{O}(M^2). \end{aligned} \quad (4.59)$$

The solutions of (1.1) thus agree with those of the incompressible model up to an error of order M^2 .

Following these theoretical results, the numerical scheme should be consistent with the limit behaviour as M tends to zero, in the sense that the discretization for the compressible Euler equations should tend to the incompressible Euler equations when the Mach number tends to zero. The key to achieve this behaviour for the presented relaxation scheme is the definition of the relaxation speeds a and b . In the former chapters several conditions are imposed on these speeds that have to be satisfied so that the scheme is stable and has the properties presented in the former sections. A suitable choice that indeed fulfils the so far stated requirements is the classical one, in which a and b are set to be equal

$$\begin{aligned} a_q^\alpha &= c^\alpha, \\ a^\alpha &= b^\alpha = \rho^\alpha c^\alpha (1 + \beta X^\alpha). \end{aligned} \quad (4.60)$$

This definition closely follows the condition (4.40) in Lemma 4. Unfortunately, this definition does not lead to an appropriate discretization, but to excessive diffusion in the low Mach limit. In order to change this behaviour the speeds have to be redefined. In this context it is important to ensure that not only the diffusion is reduced, but also that the sub-characteristic condition remains fulfilled. A suitable choice proposed by the authors of [8] is given by

$$\begin{aligned} a_q^\alpha &= \min(1, M) c^\alpha, \\ a^\alpha &= \frac{\rho^\alpha}{\min(1, M)} c^\alpha (1 + \beta X^\alpha), \\ b^\alpha &= \rho^\alpha \min(1, M) c^\alpha (1 + \beta X^\alpha). \end{aligned} \quad (4.61)$$

By this definition the speeds are rescaled in the case of small Mach numbers, i.e. for $M < 1$.

Remark 6 *In the case of Mach numbers $M \geq 1$, the relaxation speeds are equal ($a = b$) and we obtain a classical relaxation system with only one relaxation speed.*

Remark 7 *The new scaling of the relaxation speed a has the effect that the maximum wave speed increases by an order of magnitude M . As a consequence, the CFL condition (3.1) becomes stricter and the time step must be chosen smaller accordingly.*

Theorem 3 *The two-speed relaxation scheme with the relaxation speeds (4.61) is asymptotic preserving in the sense that:*

- a) *it is first order uniformly with respect to the Mach number M and*
- b) *for $M < \sqrt{k\Delta x}$ and k constant it is consistent at first order with the incompressible limit model (4.55).*

Proof. In order to prove the first statement of the theorem we evaluate the consistency error by expanding the numerical flux (3.4) in terms of M and then subtract the central flux $(F(U^L) + F(U^R))/2$.

In the low Mach limit $M \rightarrow 0$, the wave speeds σ^- and σ^+ in (2.6) tend towards infinity. Therefore it is sufficient just to consider the intermediate fluxes F^{L*} and F^{R*} for the numerical flux. In a first step of the analysis we rewrite the relaxation speeds as expansions in terms of M , so we get

$$X^\alpha = \mathcal{O}(M), \quad b^\alpha = M\bar{b}^\alpha + \mathcal{O}(M^2), \quad a^\alpha = \frac{\bar{b}^\alpha}{M}(1 + \mathcal{O}(M)) \quad (4.62)$$

with

$$\bar{b}^\alpha = \rho^\alpha c^\alpha. \quad (4.63)$$

Since

$$\bar{b}^R - \bar{b}^L = \mathcal{O}(M^2), \quad (4.64)$$

we can write \bar{b} instead of \bar{b}^L and \bar{b}^R up to errors of $\mathcal{O}(M^2)$. Expanding the intermediate states (2.14)-(2.20) in terms of M yields

$$\begin{aligned} v^* &= \frac{u^L + u^R}{2} + \frac{\pi^L - \pi^R}{2M^2\bar{b}} - \frac{\rho(Z^R - Z^L)}{2M^2\bar{b}} + \mathcal{O}(M^3), \\ \pi^{L*} &= \frac{\pi^L + \pi^R}{2} + M^2\bar{b}\frac{u^L - u^R}{2} + \frac{\bar{\rho}(Z^R - Z^L)}{2\bar{b}} + \mathcal{O}(M^3), \\ \pi^{R*} &= \frac{\pi^L + \pi^R}{2} + M^2\bar{b}\frac{u^L - u^R}{2} - \frac{\bar{\rho}(Z^R - Z^L)}{2\bar{b}} + \mathcal{O}(M^3), \\ \frac{1}{\rho^{L*}} &= \frac{1}{\rho^L} + \frac{\pi^L - \pi^R}{2\bar{b}} - \frac{\bar{\rho}(Z^R - Z^L)}{2\bar{b}} + \mathcal{O}(M^2), \\ \frac{1}{\rho^{R*}} &= \frac{1}{\rho^R} + \frac{\pi^R - \pi^L}{2\bar{b}} + \frac{\bar{\rho}(Z^R - Z^L)}{2\bar{b}} + \mathcal{O}(M^2), \\ u^{L*} &= u^L + \frac{\pi^L - \pi^R}{2\bar{b}} - \frac{\bar{\rho}(Z^R - Z^L)}{2\bar{b}} + \mathcal{O}(M^2), \\ u^{R*} &= u^R + \frac{\pi^L - \pi^R}{2\bar{b}} - \frac{\bar{\rho}(Z^R - Z^L)}{2\bar{b}} + \mathcal{O}(M^2). \end{aligned} \quad (4.65)$$

With the help of these expansions, we calculate the flux differences component by component.

i) The difference for the left intermediate flux F^{L*} in the first component writes

$$\begin{aligned}
& \rho^{L*} v^* - \frac{\rho^L u^L + \rho^R u^R}{2} \\
&= -\frac{\rho^L u^L + \rho^R u^R}{2} + \frac{1}{2\bar{b} \left(\frac{1}{\rho^L} + \frac{p^L - p^R - \bar{\rho}(Z^R - Z^L)}{2b^2} \right)} \left(\frac{p^L - p^R}{M^2} + \frac{\bar{\rho}(Z^L - Z^R)}{M^2} \right) \\
&+ \frac{u^L + u^R}{2 \left(\frac{1}{\rho^L} + \frac{p^L - p^R - \bar{\rho}(Z^R - Z^L)}{2b^2} \right)} + \mathcal{O}(M(u^L - u^R)) + \mathcal{O}(M(\pi^L - \pi^R)) \\
&+ \mathcal{O}(M\bar{\rho}(Z^L - Z^R)).
\end{aligned}$$

This difference can be further simplified. In the low Mach limit, the density is constant up to errors of $\mathcal{O}(M^2)$. Therefore we can write

$$\rho^R - \rho^L = \mathcal{O}(M^2) \quad (4.66)$$

and replace ρ^R in the difference by ρ^L . Furthermore, as stated in (4.53) and (4.54), the hydrostatic equilibrium is satisfied up to terms of order $\mathcal{O}(M^2)$ in the low Mach limit, i.e.

$$p^L - p^R + \bar{\rho}(Z^L - Z^R) = \mathcal{O}(M^2). \quad (4.67)$$

Therefore these terms disappear in the denominator. Additionally, we replace the differences between the left and right states by numerical derivatives, i.e.

$$\begin{aligned}
u^L - u^R &= -\Delta x \partial_x u + \mathcal{O}(\Delta x^2), \\
p^L - p^R &= -\Delta x \partial_x p + \mathcal{O}(\Delta x^2), \\
Z^L - Z^R &= -\Delta x \partial_x Z + \mathcal{O}(\Delta x^2).
\end{aligned} \quad (4.68)$$

Applying these simplifications results in

$$\rho^{L*} v^* - \frac{\rho^L u^L + \rho^R u^R}{2} = -\frac{\Delta x}{2} \frac{\rho^L}{\bar{b}} \left(\partial_x \frac{p}{M^2} + \bar{\rho} \partial_x \frac{Z}{M^2} \right) + \mathcal{O}(\Delta x^2) + \mathcal{O}(M\Delta x). \quad (4.69)$$

The denominator M^2 does not lead to excessive diffusion at this point, as again the hydrostatic equilibrium is fulfilled up to $\mathcal{O}(M^2)$. Analogous calculations for the right intermediate flux F^{R*} lead to

$$\rho^{R*} v^* - \frac{\rho^L u^L + \rho^R u^R}{2} = -\frac{\Delta x}{2} \frac{\rho^R}{\bar{b}} \left(\partial_x \frac{p}{M^2} + \bar{\rho} \partial_x \frac{Z}{M^2} \right) + \mathcal{O}(\Delta x^2) + \mathcal{O}(M\Delta x). \quad (4.70)$$

ii) The second component for the left flux can be expressed by

$$\begin{aligned}
& \rho^{L*} u^{L*} v^* + \frac{\pi^{L*}}{M^2} - \frac{\rho^L (u^L)^2 + \frac{\pi^L}{M^2} + \rho^R (u^R)^2 + \frac{\pi^R}{M^2}}{2} \\
&= \bar{b} \frac{u^L - u^R}{2} - \frac{\rho^L (u^L)^2 + \rho^R (u^R)^2}{2} - \frac{\bar{\rho} (Z^L - Z^R)}{2M^2} + \frac{(p^L - p^R + \bar{\rho} (Z^L - Z^R))^2}{4\bar{b}^2 M^2 \left(\frac{1}{\rho^L} + \frac{p^L - p^R - \bar{\rho} (Z^R - Z^L)}{2b^2} \right)} \\
& \quad + \frac{(p^L - p^R + \bar{\rho} (Z^L - Z^R)) u^L}{2\bar{b} M^2 \left(\frac{1}{\rho^L} + \frac{p^L - p^R - \bar{\rho} (Z^R - Z^L)}{2b^2} \right)} + \frac{(p^L - p^R + \bar{\rho} (Z^L - Z^R)) u^R}{2\bar{b} \left(\frac{1}{\rho^L} + \frac{p^L - p^R - \bar{\rho} (Z^R - Z^L)}{2b^2} \right)} \\
& \quad + \frac{u^L (u^L + u^R)}{2 \left(\frac{1}{\rho^L} + \frac{p^L - p^R - \bar{\rho} (Z^R - Z^L)}{2b^2} \right)} + \mathcal{O}(M(u^L - u^R)) + \mathcal{O}(M(\pi^L - \pi^R)) + \mathcal{O}(M\bar{\rho}(Z^L - Z^R)) \\
&= \bar{b} \frac{u^L - u^R}{2} + \rho^L u^L \frac{u^L + u^R}{2} - \rho^L u^R \frac{u^L - u^R}{2} + \rho^L u^R \frac{u^L - u^R}{2} - \frac{\rho^L (u^L)^2 + \rho^R (u^R)^2}{2} \\
& \quad + \frac{(p^L - p^R + \bar{\rho} (Z^L - Z^R)) u^L}{2\bar{b} M^2 \left(\frac{1}{\rho^L} + \frac{p^L - p^R - \bar{\rho} (Z^R - Z^L)}{2b^2} \right)} - \frac{\bar{\rho} (Z^L - Z^R)}{2M^2} + \mathcal{O}(M(u^L - u^R)) + \mathcal{O}(M(\pi^L - \pi^R)) \\
& \quad + \mathcal{O}(M\bar{\rho}(Z^L - Z^R)) \\
&= \bar{b} \frac{u^L - u^R}{2} + \rho^L u^R \frac{u^L - u^R}{2} + \frac{(p^L - p^R + \bar{\rho} (Z^L - Z^R)) u^L}{2\bar{b} M^2 \left(\frac{1}{\rho^L} + \frac{p^L - p^R - \bar{\rho} (Z^R - Z^L)}{2b^2} \right)} - \frac{\bar{\rho} (Z^L - Z^R)}{2M^2} \\
& \quad + \mathcal{O}(M(u^L - u^R)) + \mathcal{O}(M(\pi^L - \pi^R)) + \mathcal{O}(M\bar{\rho}(Z^L - Z^R)) \\
&= -\frac{\Delta x}{2} (\bar{b} + \rho^L u^R) \partial_x u - \frac{\Delta x}{2} \frac{\rho^L u^L}{\bar{b}} \left(\partial_x \frac{p}{M^2} + \bar{\rho} \partial_x \frac{Z}{M^2} \right) + \frac{\Delta x}{2} \bar{\rho} \partial_x \frac{Z}{M^2} \\
& \quad + \mathcal{O}(\Delta x^2) + \mathcal{O}(M\Delta x)
\end{aligned}$$

and for the right flux by

$$\begin{aligned}
& \rho^{R*} u^{R*} v^* + \frac{\pi^{R*}}{M^2} - \frac{\rho^L (u^L)^2 + \frac{\pi^L}{M^2} + \rho^R (u^R)^2 + \frac{\pi^R}{M^2}}{2} \\
&= -\frac{\Delta x}{2} (\bar{b} + \rho^R u^L) \partial_x u - \frac{\Delta x}{2} \frac{\rho^R u^R}{\bar{b}} \left(\partial_x \frac{p}{M^2} + \bar{\rho} \partial_x \frac{Z}{M^2} \right) - \frac{\Delta x}{2} \bar{\rho} \partial_x \frac{Z}{M^2} \\
& \quad + \mathcal{O}(\Delta x^2) + \mathcal{O}(M\Delta x).
\end{aligned}$$

In this flux difference, the new scaling of the relaxation speeds defined in (4.61) unfolds its importance. Clearly, the viscosity on the velocity, represented by the first term, is independent of the Mach number and therefore does not increase in the low Mach limit. With the classical scaling (4.60), on the other hand, this term would have the size $\mathcal{O}(1/M)$ leading to excessive diffusion for low Mach numbers. While a Mach number dependence in the first term would be problematic, it is not in the second term due to (4.67). The remaining third term containing the derivative of the gravitational potential, which also depends on $1/M^2$, cancels out with the gravitational source term (3.6) in the relaxation scheme.

iii) For the difference in the third component, similar steps for the left flux result in

$$\begin{aligned}
& \left(\left(\frac{1}{2} M^2 \rho^{L*} (u^{L*})^2 + \rho^{L*} e^{L*} \right) + \pi^{L*} \right) v^* - \frac{(E^L + p^L)u^L + (E^R + p^R)u^R}{2} \\
&= \rho^L u^R \frac{e^L - e^R}{2} + u^R \frac{p^L - p^R}{2} + \frac{\rho^L e^L + p^L}{2\bar{b}} \frac{p^L - p^R + \bar{\rho}(Z^L - Z^R)}{M^2} \\
&\quad + \mathcal{O}(M(u^L - u^R)) + \mathcal{O}(M(\pi^L - \pi^R)) + \mathcal{O}(M\bar{\rho}(Z^L - Z^R)) \\
&= -\frac{\Delta x}{2} \rho^L u^R \partial_x e - \frac{\Delta x}{2} u^R \partial_x p - \frac{\Delta x}{2} \frac{\rho^L e^L + p^L}{\bar{b}} \left(\partial_x \frac{p}{M^2} + \partial \frac{Z}{M^2} \right) + \mathcal{O}(\Delta x^2) + \mathcal{O}(M\Delta x).
\end{aligned}$$

and for the right flux in

$$\begin{aligned}
& \left(\left(\frac{1}{2} M^2 \rho^{R*} (u^{R*})^2 + \rho^{R*} e^{R*} \right) + \pi^{R*} \right) v^* - \frac{(E^L + p^L)u^L + (E^R + p^R)u^R}{2} \\
&= \frac{\Delta x}{2} \rho^R u^L \partial_x e + \frac{\Delta x}{2} u^L \partial_x p - \frac{\Delta x}{2} \frac{\rho^R e^R + p^R}{\bar{b}} \left(\partial_x \frac{p}{M^2} + \partial \frac{Z}{M^2} \right) + \mathcal{O}(\Delta x^2) + \mathcal{O}(M\Delta x).
\end{aligned}$$

The expansions for all three components are first-order uniformly in M . It is particularly important that the viscosity on the velocity u is independent of M .

The result of the first statement can now be used to prove the second statement of the theorem. We have proven that the solution $w_{M,\Delta x}$ of the relaxation scheme is consistent with the exact solution w_M of the dimensionless Euler equations (1.1) up to order $\mathcal{O}(\Delta x)$ independent of the Mach number, i.e.

$$w_{M,\Delta x} - w_M = \mathcal{O}(\Delta x). \quad (4.71)$$

Additionally, we can deduce from the system (4.59) that w_M is consistent with the solution w of the incompressible Euler equations up to order $\mathcal{O}(M^2)$, i.e.

$$w_M - w = \mathcal{O}(M^2). \quad (4.72)$$

Combining (4.71) and (4.72) with the condition that $M^2 = \mathcal{O}(\Delta x)$ finally results in

$$w_{M,\Delta x} - w = \mathcal{O}(\Delta x) \quad (4.73)$$

and therefore meets the second statement of the theorem. \square

4.5 Well-balanced property

As explained in the introduction, the well-balanced property is important for solving problems close to hydrostatic equilibrium. In a first step, we will show that the approximate Riemann solver satisfies this property. Building on this, we will then prove in the second step that the entire scheme has this property.

Lemma 6 *Assume two given states at equilibrium W^L and W^R satisfy*

$$u^L = u^R = 0, \quad (4.74)$$

$$p^R - p^L + \bar{\rho}(W^L, W^R)(\Phi^R - \Phi^L) = 0. \quad (4.75)$$

Then the approximate Riemann solver $W_{\mathcal{R}}$ preserves the steady state, i.e.

$$W_{\mathcal{R}}(x/t, W^L, W^R) = \begin{cases} W^L & \text{if } x/t < 0, \\ W^R & \text{if } x/t > 0. \end{cases} \quad (4.76)$$

Proof. The result directly follows from the definition of the intermediate states given in (2.14)-(2.23). Consider the intermediate state v^* . Since we start at equilibrium, we can replace the relaxation variables by their corresponding original variables. Using the conditions (4.74)-(4.75) results in

$$v^* = \frac{1}{b^L + b^R} (Mb^L u^L + Mb^R u^R + p^L - p^R - \bar{\rho}(W^L, W^R) (\Phi^R - \Phi^L)) = 0.$$

Similar calculations for the other intermediate states complete the proof. \square

Lemma 6 is rather general, as it assumes that the conditions in (4.74) and (4.75) are satisfied. Clearly, these conditions depend on the definition of the $\bar{\rho}$ -function. For a simple definition like the arithmetic mean, which is not adjusted to the underlying hydrostatic equilibrium, the scheme maintains the equilibrium to second order [16]. Since we are free to define $\bar{\rho}$ we can adjust it to the hydrostatic equilibrium and maintain it even up to machine precision. The only limiting requirements for $\bar{\rho}$ that have to be considered are the consistency property

$$\rho^L = \rho^R = \rho \quad \Rightarrow \quad \bar{\rho}(W^L, W^R) = \rho \quad (4.77)$$

and the symmetry property

$$\bar{\rho}(W^L, W^R) = \bar{\rho}(W^R, W^L). \quad (4.78)$$

The following lemma describes the adjusted definitions for isothermal, incompressible and polytropic equilibria. These definitions were already described in [16].

Lemma 7

i) Let W^L and W^R be two states satisfying the isothermal equilibrium

$$\begin{cases} u^L = u^R = 0, \\ \rho^{L,R} = \exp \frac{C - \Phi^{L,R}}{K}, \\ p^{L,R} = K \exp \frac{C - \Phi^{L,R}}{K}, \end{cases} \quad (4.79)$$

with $K > 0$ and $C \in \mathbb{R}$. If the function $\bar{\rho}$ is defined by

$$\bar{\rho}(W^L, W^R) = \begin{cases} \frac{\rho^R - \rho^L}{\ln(\rho^R) - \ln(\rho^L)} & \text{if } \rho^L \neq \rho^R, \\ \rho^L & \text{if } \rho^L = \rho^R, \end{cases} \quad (4.80)$$

then the approximate Riemann solver $W_{\mathcal{R}}$ preserves the steady state.

ii) Let W^L and W^R be two states satisfying the incompressible equilibrium

$$\begin{cases} u^L = u^R = 0, \\ \rho^L = \rho^R, \\ p^L + \rho^L \Phi^L = p^R + \rho^R \Phi^R. \end{cases} \quad (4.81)$$

If the function $\bar{\rho}$ satisfies the consistency condition (4.77), then the approximate Riemann solver $W_{\mathcal{R}}$ preserves the steady state.

iii) Let W^L and W^R be two states satisfying the polytropic equilibrium

$$\begin{cases} u^L = u^R = 0, \\ \rho^{L,R} = \left(\frac{\Gamma-1}{\Gamma K} (C - \Phi^{L,R}) \right)^{\frac{\Gamma}{\Gamma-1}}, \\ p^{L,R} = K^{\frac{1}{1-\Gamma}} \left(\frac{\Gamma-1}{\Gamma} (C - \Phi^{L,R}) \right)^{\frac{\Gamma}{\Gamma-1}}, \end{cases} \quad (4.82)$$

with $\Gamma \in (0, 1) \cup (1, +\infty)$, $K > 0$ and $C \in \mathbb{R}$. If the function $\bar{\rho}$ is defined by

$$\bar{\rho}(W^L, W^R) = \begin{cases} \frac{\Gamma-1}{\Gamma} \frac{(\rho^R)^\Gamma - (\rho^L)^\Gamma}{(\rho^R)^{\Gamma-1} - (\rho^L)^{\Gamma-1}} & \text{if } \rho^L \neq \rho^R, \\ \rho^L & \text{if } \rho^L = \rho^R, \end{cases} \quad (4.83)$$

then the approximate Riemann solver $W_{\mathcal{R}}$ preserves the steady state.

Proof. In order to prove this lemma it is sufficient to show that with the explicit definition of $\bar{\rho}$ the conditions (4.74) and (4.75) are satisfied. If so, we can use lemma 6 and the proof is complete. Using the definitions of the isothermal equilibrium states, we can determine the following differences

$$\begin{aligned} \Phi^R - \Phi^L &= K(\ln(\rho^R) - \ln(\rho^L)), \\ p^R - p^L &= K(\rho^R - \rho^L). \end{aligned}$$

By inserting these differences together with $\bar{\rho}$ defined by (4.80) into equation (4.75), it becomes clear that this condition is satisfied. Together with the velocities, which are zero, lemma 6 can be applied and the proof of i) is complete. The proofs for incompressible and polytropic equilibria work in the same way. For more details we refer the reader to [16]. \square

Remark 8 To ensure the exact preservation of steady states at rest, it is important to consider the following two points in the implementation:

1. The comparative operators in the approximate Riemann solver (3.4) must be adjusted to the definition of the sign function in the programming language used. The choice provided here is adapted to $\text{sign}(0) = 1$.
2. The implementation of the classical definition of the logarithmic mean can lead to problems if left and right input are very close. Ismail and Roe provide an alternative way of implementation in [19], which avoids this problem.

In practical applications, e.g. in astrophysics, the hydrostatic states are often just available as discrete data generated by previously performed simulations. The following lemma provides an approach to maintain these hydrostatic equilibria as well.

Lemma 8 Let W^L and W^R be two states satisfying some hydrostatic equilibrium

$$\begin{cases} u^L = u^R = 0, \\ \rho^{L,R} = \rho_{hs}^{L,R}, \\ p^{L,R} = p_{hs}^{L,R}, \end{cases} \quad (4.84)$$

with ρ_{hs} and p_{hs} given hydrostatic states. If the function $\bar{\rho}$ is defined by

$$\bar{\rho}(W^L, W^R) = \frac{1}{2}(\rho^L + \rho^R) \quad (4.85)$$

and the difference of the gravitational potential in the intermediate states is approximated by

$$Z^R - Z^L \approx -\frac{p_{hs}^R - p_{hs}^L}{\frac{1}{2}(\rho_{hs}^L + \rho_{hs}^R)}, \quad (4.86)$$

then the approximate Riemann solver $W_{\mathcal{R}}$ preserves the steady state.

Proof. As can be seen in the proof of lemma 7 it is sufficient to show that the conditions (4.74) and (4.75) are fulfilled so that lemma 6 can be applied. In order to do so we plug the states from (4.84) and the approximation (4.86) into (4.75) and use definition (4.85) for $\bar{\rho}$. This results in

$$p_{hs}^R - p_{hs}^L - \frac{1}{2}(\rho_{hs}^L + \rho_{hs}^R) \frac{p_{hs}^R - p_{hs}^L}{\frac{1}{2}(\rho_{hs}^L + \rho_{hs}^R)} = 0. \quad (4.87)$$

□

Now that it has been shown that the approximate Riemann solver satisfies the well-balanced property, it remains to show that the entire scheme does so as well.

Theorem 4 *Let us consider an initial data W_i^0, W_{i+1}^0 that satisfies*

$$\begin{aligned} u_i^0 &= u_{i+1}^0 = 0, \\ \frac{1}{\Delta x}(p_{i+1}^0 - p_i^0) + \bar{\rho}(W_i^0, W_{i+1}^0) \frac{\Phi_{i+1} - \Phi_i}{\Delta x} &= 0. \end{aligned} \quad (4.88)$$

Then the updated state W^{n+1} stays at rest, and thus satisfies $W_i^{n+1} = W_i^n$ for all $i \in \mathbb{Z}$.

Proof. Since both conditions (4.74) and (4.75) of lemma 6 are fulfilled, the approximate Riemann solver stays at rest. The updated state W_i^1 at time $t = \Delta t$ is in essence the sequence of approximate Riemann solvers. Since the approximate Riemann solver is at rest, it directly follows $W_i^1 = W_i^0$ for all $i \in \mathbb{Z}$. □

5 Second order extension

In this section we give a possible extension of the proposed scheme to second order in space. We use a linear reconstruction in the primitive variables $W^p = (\rho, \mathbf{u}, p)$. In order to obtain the values $W_{i-1/2}^+$ and $W_{i+1/2}^-$ at the interfaces, we evaluate the function

$$W^p(x) = W_i^p + \sigma(x - x_i) \quad (5.1)$$

in each cell \mathcal{C}_i at its boundaries $x_{i-1/2}$ and $x_{i+1/2}$. The slope σ depends on the neighbouring cells and is computed for each primitive variable separately. In order to guarantee that the reconstructed values for the density and internal energy remain positive, which is essential for

the positivity property given by the lemmata 3 and 4, we use an approach introduced by Berthon in [6]. Then the slopes are defined by

$$\begin{aligned}\sigma^\rho &= \rho_i \max \left(-1, \min \left(1, \frac{\bar{\sigma}^\rho}{\rho_i} \right) \right), \\ \boldsymbol{\sigma}^u &= \omega \bar{\boldsymbol{\sigma}}^u, \\ \sigma^p &= p_i \max \left(-1, \min \left(1, \frac{\bar{\sigma}^p}{p_i} \right) \right),\end{aligned}\tag{5.2}$$

with

$$\bar{\sigma} = \text{minmod} \left(\frac{W_i^p - W_{i-1}^p}{\Delta x}, \frac{W_{i+1}^p - W_i^p}{\Delta x} \right)\tag{5.3}$$

and

$$\begin{aligned}\omega &= \min(1, \bar{\omega}), \\ \bar{\omega} &= \begin{cases} \frac{\sigma^\rho(\mathbf{u}_i \cdot \bar{\boldsymbol{\sigma}}^u) + \sqrt{\frac{(\gamma-1)(\sigma^\rho)^2(\mathbf{u}_i \cdot \bar{\boldsymbol{\sigma}}^u)^2 + 2\rho_i p_i}{\gamma-1}}}{2\rho_i \|\bar{\boldsymbol{\sigma}}^u\|^2}, & \text{if } \bar{\boldsymbol{\sigma}}^u \neq 0 \\ 1, & \text{if } \bar{\boldsymbol{\sigma}}^u = 0. \end{cases}\end{aligned}\tag{5.4}$$

Additionally, we also want to preserve the well-balanced property for the second-order scheme. To achieve this, we adjust the pressure slope by using a hydrostatic reconstruction [21, 29, 30]. Instead of directly using the pressure values of the neighbouring cells, one first applies the transformations

$$\begin{aligned}q_{i-1} &= p_{i-1} - \bar{\rho}(W_{i-1}, W_i)(\Phi_i - \Phi_{i-1}), \\ q_{i+1} &= p_{i+1} + \bar{\rho}(W_i, W_{i+1})(\Phi_{i+1} - \Phi_i),\end{aligned}\tag{5.5}$$

and then computes the slope for the pressure by

$$\bar{\sigma}^p = \text{minmod} \left(\frac{p_i - q_{i-1}}{\Delta x}, \frac{q_{i+1} - p_i}{\Delta x} \right).\tag{5.6}$$

In the case of hydrostatic equilibrium, the slope becomes zero and the interface values for the pressure thus reduce to the cell averages. The approximate Riemann solver then stays at rest due to lemma 6 and all results of the former chapter about well-balancing remain valid for the second order scheme.

The second order scheme remains asymptotic preserving since the differences in (4.68) are due to the linear reconstruction of order $\mathcal{O}(\Delta x^2)$. Therefore, the scheme is second order uniformly in M . The steps of proof of the second part of theorem 3 remain unchanged under the new condition $M < \sqrt{k\Delta x^2}$.

6 Numerical results

In this chapter we numerically investigate the theoretical properties of the relaxation scheme presented in the previous chapters. The approximate Riemann solver in the scheme is equipped with the intermediate states defined in (2.14)-(2.23) and the relaxation speeds (4.61) with $\beta = 1.1$. Various definitions are used for the $\bar{\rho}$ -function. Definition (4.80) is used by default. If a different choice is made, this is indicated in the respective test. The second order spatial scheme is combined with a third order Runge Kutta method [27] for time integration. For all test set-ups we assume an ideal gas law $p = (\gamma - 1)\rho e$.

6.1 Accuracy

In a first numerical test, which is suggested by [33], we investigate the experimental order of convergence of the relaxation scheme presented. For the Euler equations (1.1) on the domain $[0, 1]^2$ with a linear gravitational potential $\Phi(x, y) = x + y$, one possible exact solution is defined by

$$\begin{aligned} \rho(x, y, t) &= 1 + 0.2 \sin(\pi(x + y - t(u_{1_0} + u_{2_0}))), \\ \mathbf{u}(x, y, t) &= (u_{1_0}, u_{2_0}), \\ p(x, y, t) &= 4.5 + (u_{1_0} + u_{2_0})t - (x + y) + 0.2 \cos((\pi(x + y - (u_{1_0} + u_{2_0})t)) / \pi), \end{aligned} \tag{6.1}$$

with $u_{1_0} = u_{2_0} = 20$ and $p_0 = 4.5$. The exact solution is also used for the boundary conditions. The adiabatic coefficient is set to $\gamma = 5/3$. We compare the numerical and exact solutions at final time $T = 0.01$. The resulting L^1 errors and experimental orders of convergence can be found in Table 1. As expected, we obtain orders of convergence of nearly two. Without the use of limiters full second order is reached.

N	$L^1(\rho)$	$EOC(\rho)$	$L^1(\rho u_1)$	$EOC(\rho u_1)$	$L^1(\rho u_2)$	$EOC(\rho u_2)$	$L^1(E)$	$EOC(E)$
32	7.26E-04	-	1.45E-02	-	1.45E-02	-	2.90E-01	-
64	1.97E-04	1.88	3.93E-03	1.88	3.93E-03	1.88	7.87E-02	1.88
128	5.22E-05	1.92	1.04E-03	1.92	1.04E-06	1.92	2.08E-02	1.92
256	1.37E-05	1.92	2.73E-04	1.93	2.73E-04	1.93	5.47E-03	1.93
512	3.60E-06	1.94	7.10E-05	1.94	7.10E-05	1.94	1.42E-03	1.95

Table 1 L^1 errors and experimental orders of convergence

6.2 Strong rarefaction test

In this section we want to numerically verify the theoretical results of chapter 4.3, i.e. the positivity of density and internal energy. One suitable test for which density and pressure become very small is the 1-2-0-3 strong rarefaction test [30]. In this test set-up, two rarefaction waves are launched in x-direction on top of an isothermal atmosphere. Therefore, on the domain $[0, 1]^2$ the density ρ and pressure p are initially defined by (4.79) with the constants $C = -0.01$ and $K = \gamma - 1$, an adiabatic coefficient $\gamma = 1.4$ and a quadratic gravitational potential $\Phi(x, y) = \frac{1}{2}[(x - 0.5)^2 + (y - 0.5)^2]$. The initial velocities are set to

$$u_1 = \begin{cases} -2, & x < 0.5, \\ 2, & x \geq 0.5, \end{cases} \quad \text{and} \quad u_2 = 0. \tag{6.2}$$

One slice along the x -axis of the numerical solution at final time $T = 0.1$ computed on a 128×128 grid by our relaxation scheme is presented in Fig. 2. Although the values for density and total pressure become very small during the simulation, they always remain positive. This outcome underlines the theoretical results stated in lemmata 3 and 4.

6.3 Isothermal atmosphere

The following set-up is taken from [11]. The aim of this experiment is to illustrate the exact preservation of an isothermal equilibrium. We consider the gravitational potential

$$\Phi(x, y) = x + y. \tag{6.3}$$

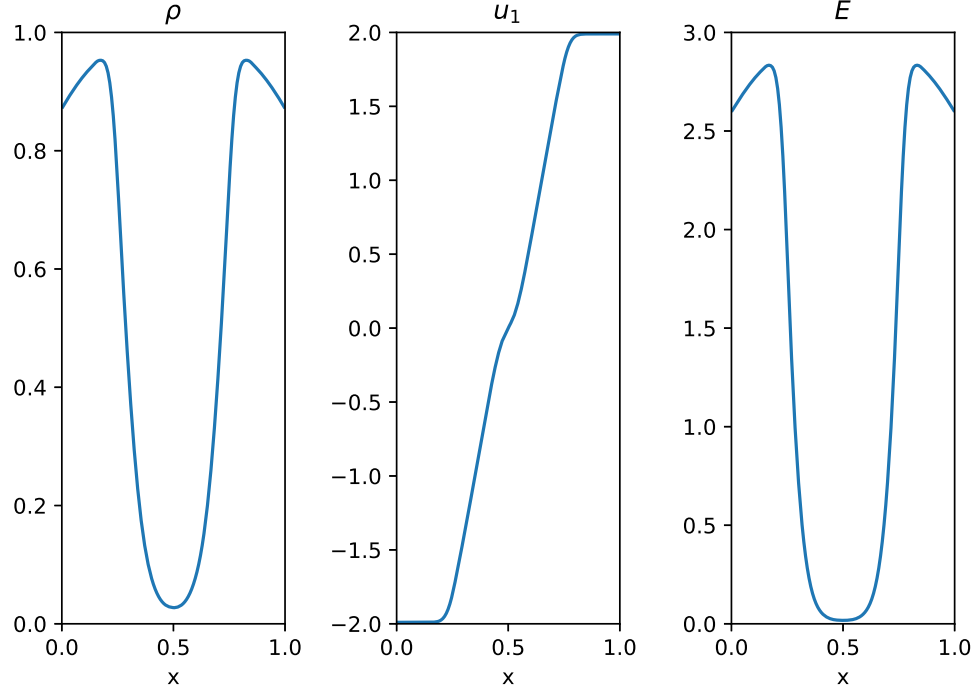


Fig. 2 Numerical solution for density, velocity and total energy at final time $T = 0.1$

The initial conditions on the domain $[0, 1]^2$ are given by

$$\begin{aligned}
 \rho(x, y, 0) &= \rho_0 \exp(-\rho_0 g(x + y)/p_0), \\
 \mathbf{u}(x, y, 0) &= 0, \\
 p(x, y, 0) &= p_0 \exp(-\rho_0 g(x + y)/p_0),
 \end{aligned} \tag{6.4}$$

with the parameters $\rho_0 = 1.21$, $p_0 = 1$ and $g = 1$. In this test we set $\gamma = 1.4$. The solution should be preserved up to any final time. Here we choose $T = 1.0$. Since the solution is in hydrostatic equilibrium, the choice of the $\bar{\rho}$ -average plays an important role. As this is an isothermal equilibrium, we use for $\bar{\rho}$ the definition (4.80). The L^1 error between the approximated solution and the exact solution is given in Table 2 and is in the order of magnitude of the machine accuracy.

N	$L^1(\rho)$	$L^1(\rho u_1)$	$L^1(\rho u_2)$	$L^1(E)$
32	8.95E-17	5.21E-16	5.21E-16	4.18E-16
64	1.73E-16	1.62E-16	1.62E-16	7.24E-16
128	3.40E-16	3.47E-16	3.47E-16	1.63E-15
256	6.30E-16	6.89E-16	6.89E-16	3.46E-15
512	1.22E-15	1.54E-15	1.54E-15	7.43E-15

Table 2 L^1 errors for an isothermal atmosphere

6.4 General steady state

In practice, steady states that do not belong to the class of polytropic equilibria can also occur. In order to investigate the behaviour of the well-balancing mechanism for these cases, we now apply the scheme to a general steady state. We take the initial conditions from the set-up in chapter 6.1 and set the initial velocities u_{1_0} and u_{2_0} to zero. Then it is easy to check that the initial data is in hydrostatic equilibrium.

In a first step, we use the $\bar{\rho}$ -average tuned to isothermal equilibria (4.80) and compute the solution at final time $T = 1$. As expected, the L^1 error shown in Table 3 is now no longer in the order of magnitude of the machine accuracy, but the hydrostatic equilibrium is still preserved up to second order. This result remains true even if we use a constant reconstruction and consequently a first order scheme. As the convergence rates in Table 4 show, the hydrostatic equilibrium is maintained up to second order despite the constant reconstruction. Mathematically, this can be explained by the fact that equation (4.88) is satisfied up to second order.

N	$L^1(\rho)$	$EOC(\rho)$	$L^1(\rho u_1)$	$EOC(\rho u_1)$	$L^1(\rho u_2)$	$EOC(\rho u_2)$	$L^1(E)$	$EOC(E)$
32	9.43E-06	-	1.36E-05	-	1.36E-05	-	5.08E-05	-
64	2.35E-06	2.01	3.43E-06	1.99	3.43E-06	1.99	1.26E-05	2.01
128	5.88E-07	2.00	8.60E-07	2.00	8.60E-07	2.00	3.14E-06	2.01
256	1.47E-07	2.00	2.16E-07	1.99	2.16E-07	1.99	7.85E-07	2.00
512	3.69E-08	2.00	5.42E-08	2.00	5.42E-08	2.00	1.97E-07	2.00

Table 3 L^1 errors and experimental orders of convergence of the second order scheme for a general steady state using the $\bar{\rho}$ -average (4.80)

N	$L^1(\rho)$	$EOC(\rho)$	$L^1(\rho u_1)$	$EOC(\rho u_1)$	$L^1(\rho u_2)$	$EOC(\rho u_2)$	$L^1(E)$	$EOC(E)$
32	9.74E-06	-	1.40E-05	-	1.40E-05	-	5.15E-05	-
64	2.39E-06	2.03	3.48E-06	2.01	3.48E-06	2.01	1.27E-05	2.02
128	5.93E-07	2.01	8.67E-07	2.01	8.67E-07	2.01	3.15E-06	2.01
256	1.48E-07	2.00	2.17E-07	2.00	2.17E-07	2.00	7.86E-07	2.00
512	3.70E-08	2.00	5.43E-08	2.00	5.43E-08	2.00	1.97E-07	2.00

Table 4 L^1 errors and experimental orders of convergence of the first order scheme for a general steady state using the $\bar{\rho}$ -average (4.80)

Let us now assume that we know the hydrostatic equilibrium a priori and it is given as discrete data for the density and pressure. In this case, the approach described in lemma 8 should be able to maintain this particular hydrostatic equilibrium up to machine precision. In order to check this, we set the values ρ_{hs} and p_{hs} equal to the initial values for density respective pressure. The L^1 errors in Table 5 show that the hydrostatic equilibrium is maintained up to machine precision.

6.5 Perturbation of an isothermal atmosphere

One main advantage of well-balanced schemes is their ability to resolve small perturbations on the hydrostatic equilibrium even on coarse grids. It is precisely this effect that we are

N	$L^1(\rho)$	$L^1(\rho u_1)$	$L^1(\rho u_2)$	$L^1(E)$
32	6.54E-17	9.10E-16	9.10E-16	1.33E-15
64	1.85E-16	1.95E-15	1.95E-15	4.78E-15
128	2.98E-16	4.78E-15	4.78E-15	8.97E-15
256	6.25E-16	8.32E-16	8.32E-16	2.04E-14
512	1.25E-15	1.83E-14	1.83E-14	4.24E-14

Table 5 L^1 errors for a general steady state using the approach for a-priori known hydrostatic equilibria from lemma 8

investigating with the following test. For this purpose, we take the initial values from section 6.3, which are in hydrostatic equilibrium, and add a perturbation on the pressure

$$p(x, y, 0) = \rho_0 \exp(-\rho_0 g(x + y)/p_0) + \eta \exp(-100\rho_0 g((x - 0.3)^2 + (y - 0.3)^2)/p_0). \quad (6.5)$$

The strength of the perturbation is controlled by the parameter η . The numerical solutions are computed on a 64×64 mesh up to a final time $t = 0.15$. In order to investigate the well-balancing effect, we compare the results of our well-balanced scheme with a non-well-balanced scheme. The non-well-balanced scheme uses a Rusanov flux in combination with a linear reconstruction limited by the minmod limiter.

The numerical solutions of the two schemes for a large perturbation $\eta = 0.1$ are illustrated in the two upper plots of Fig. 3. Looking at the two solutions, it can be said that they are visually very similar. Both methods are capable of resolving the perturbation well. For a significantly smaller perturbation ($\eta = 1\text{E}-10$), the situation is completely different. While our well-balanced relaxation scheme is still capable to resolve the perturbation (in fact one cannot see any difference in the resolution in comparison to the larger perturbation), the non-well-balanced scheme completely destroys the structure of the initial pressure pulse. This underlines the functionality of the well-balanced mechanism in the relaxation scheme and also demonstrates the importance of this property for problems close to hydrostatic equilibrium.

6.6 Stationary vortex in a gravitational field

In this section, we investigate the effect of the new scaling of the relaxation speeds a and b for problems with low Mach numbers. Therefore we compare the two-speed relaxation scheme using the speeds defined in (4.61) with the one-speed relaxation scheme using the speeds (4.60).

As a test, we use a version of the Gresho vortex modified for the Euler equations with a gravitational source term that was already given in [30]. The density in this set-up is defined by

$$\rho = \exp\left(-\frac{\Phi}{RT}\right). \quad (6.6)$$

The rest of the initial data is given in radial coordinates (r, θ) . The velocity field has the form

$$u_\theta(r) = \frac{1}{u_r} \begin{cases} 5r, & r \leq 0.2 \\ 2 - 5r, & 0.2 < r \leq 0.4 \\ 0, & r > 0.4 \end{cases} \quad (6.7)$$

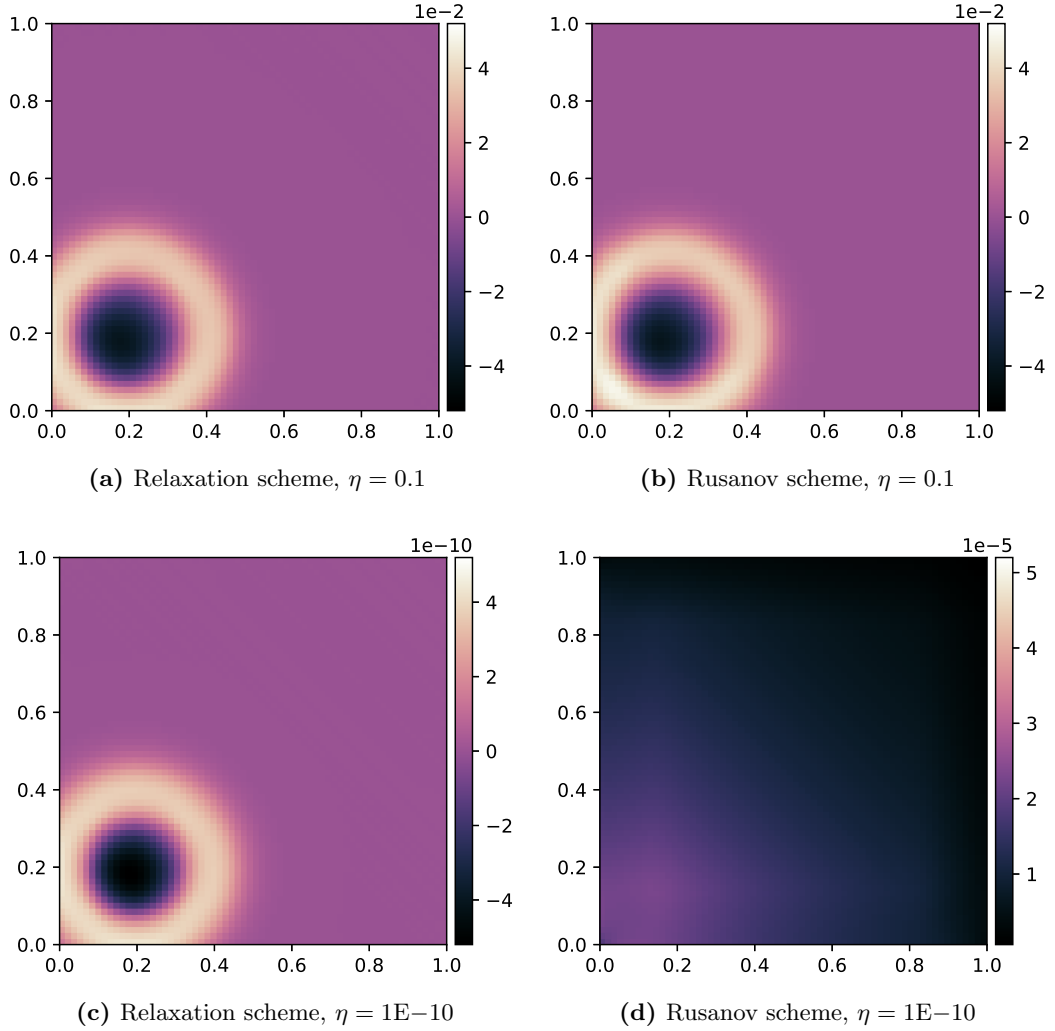


Fig. 3 Pressure perturbation of an isothermal atmosphere at $t = 0.15$

and the gravitational potential is defined by

$$\Phi(r) = \begin{cases} 12r^2, & r \leq 0.2 \\ 0.5 - \ln(0.2) + \ln(r), & 0.2 < r \leq 0.4 \\ \ln(2) - 0.5\frac{r_c}{r_c-0.4} + 2.5\frac{r_c}{r_c-0.4}r - 1.25\frac{1}{r_c-0.4}r^2, & 0.4 < r \leq r_c \\ \ln(2) - 0.5\frac{r_c}{r_c-0.4} + 1.25\frac{r_c^2}{r_c-0.4}, & r > r_c. \end{cases} \quad (6.8)$$

The pressure p is departed into a hydrostatic pressure p_0 and a pressure p_2 associated with the centrifugal forces and given by $p = p_0 + M^2 p_2$, where $p_0 = RT\rho$ and

$$p_2(r) = \frac{RT}{u_r^2} \begin{cases} p_{21}(r), & r \leq 0.2 \\ p_{21}(0.2) + p_{22}(r), & 0.2 < r \leq 0.4 \\ p_{21}(0.2) + p_{22}(0.4), & 0.4 < r \leq r_c \end{cases} \quad (6.9)$$

with

$$\begin{aligned}
 p_{21}(r) &= \left(1 - \exp\left(-12.5 \frac{r^2}{RT}\right) \right), \\
 p_{22}(r) &= \frac{1}{(1 - M^2)(1 - 0.5M^2)} \exp\left(\frac{-0.5 + \ln(0.2)}{RT}\right) \\
 &\quad \left(r^{-\frac{1}{RT}} (M^4(r(10 - 12.5r) - 2) - 4 + M^4(r(12.5r - 20) + 6)RT) \right. \\
 &\quad \left. + \exp\left(\frac{-\ln(0.2)}{RT}\right) (4 - 2.5M^4RT + 0.5M^4) \right).
 \end{aligned}$$

The reference values are given by $u_r = 2 \cdot 0.2 \cdot \pi$ and $RT = 1/M^2$. We choose $\gamma = 5/3$ for the adiabatic coefficient. The spatial domain is $D = [0, 1]^2$ and has periodic boundary conditions. The computations are carried out on a 40×40 grid until a final time $T = 1$, which corresponds to one turn of the vortex. We solve this initial value problem for various maximum Mach numbers M using the two different schemes. The solutions generated by the one-speed relaxation scheme are depicted in the top row of Fig. 4, while the solutions computed by the two-speed relaxation scheme are shown in the bottom row. It becomes clear that for decreasing Mach numbers, the vortex in the upper row smears out very quickly and even loses its shape completely. The vortex produced by the two-speed scheme in the lower row, on the other hand, retains its shape regardless of the Mach number, so that no difference is visually discernible.

This outcome can be explained by the theoretical results from chapter 4.4. While the diffusion for the one-speed scheme increases for decreasing Mach numbers, the use of two relaxation speeds, as shown in the proof of theorem 3, results in a Mach number independent diffusion. Further evidence for this behaviour can be found in the analysis of the kinetic energy. Table 6 contains the percentages of kinetic energy compared to the initial value after one full turnover. The final amount of kinetic energy in the solutions of the one-speed scheme strongly decreases for decreasing Mach numbers. In contrast, the asymptotic preserving two-speed scheme is able to keep the loss almost constant at 14%, regardless of the Mach number.

scheme	$M = 0.1$	$M = 0.01$	$M = 0.001$
1-speed	62.74	47.49	50.08
2-speed	86.03	86.00	85.99

Table 6 Percentage of kinetic energy compared to the initial value after one full turnover ($T = 1$) for the stationary vortex in a gravitational field

7 Conclusion

The proposed scheme extends the two-speed relaxation approach to the full Euler equations with a gravitational source term. In order to preserve steady states at rest, a well-balancing mechanism is installed in the approximate Riemann solver. The resulting scheme is provably asymptotic preserving and maintains all hydrostatic equilibria up to second order, certain families and a-priori known equilibria even up to machine precision. The approximate Riemann solver is positivity preserving, entropy satisfying and prevents the occurrence of checkerboard modes in the velocity and pressure variables. The properties of the method proven in theory are

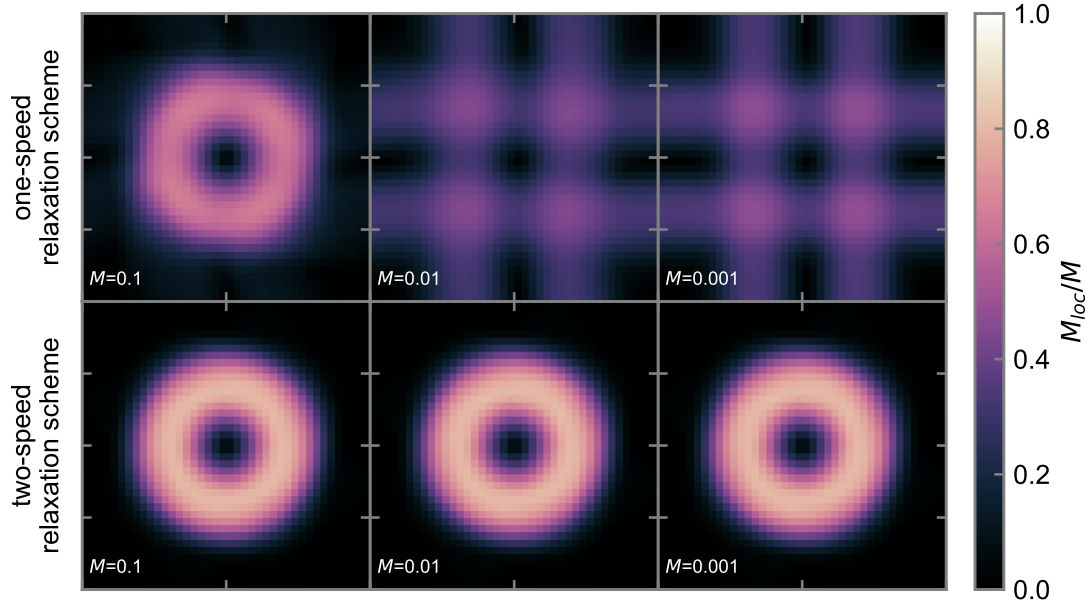


Fig. 4 Numerical solutions for different maximum Mach numbers M after one full turnover. The local Mach number relative to the respective M is color coded

substantiated in numerical tests. Further steps may be the development of an IMEX scheme based on the herein presented full time explicit scheme in order to overcome the severe time step restriction for problems with very low Mach numbers, and the extension to other PDE systems like the MHD equations.

Acknowledgements

The authors thank Jonas Berberich for his comments on the well-balancing of a-priori known hydrostatic equilibria. We acknowledge the use of the *Seven-League Hydro Code* (<https://slh-code.org>) for our numerical experiments. Claudius Birke acknowledges the support by the German Research Foundation (DFG) under the project no. 418833237. All three authors acknowledge the project "Bayerisch-Französische Hochschulzentrum FK40_2019" which supported this work.

Appendix

A Limit equations for ideal gas laws

In chapter 4.4, the limit equations are derived. In the following, the calculations to achieve equation (4.56) for the case of an ideal gas law $p = (\gamma - 1)\rho e$ are explained in more detail. We

start with the third equation in (4.55) for arbitrary pressure laws

$$\partial_t e_0 + \mathbf{u}_0 \cdot \nabla e_0 + \frac{1}{\rho_0} \nabla \cdot (p_0 \mathbf{u}_0) = -\mathbf{u}_0 \cdot \nabla \Phi.$$

Under the assumption of an ideal gas law, the internal energy is defined by

$$e = \frac{p}{(\gamma - 1)\rho}.$$

Inserting this formula in the equation above we gain

$$\frac{1}{\gamma - 1} \partial_t \frac{p_0}{\rho_0} + \frac{\mathbf{u}_0}{\gamma - 1} \cdot \nabla \frac{p_0}{\rho_0} + \frac{1}{\rho_0} \nabla \cdot (p_0 \mathbf{u}_0) + \mathbf{u}_0 \cdot \nabla \Phi = 0.$$

From (4.53), we know that ρ_0 and p_0 are time-independent, which is why the time derivative term can be omitted. Additionally, we use equation (4.53) and replace the gravitational potential term, which in combination with the product rule results in

$$\frac{\mathbf{u}_0}{\gamma - 1} \cdot \nabla \frac{p_0}{\rho_0} + \frac{p_0}{\rho_0} \nabla \cdot \mathbf{u}_0 = 0.$$

By applying the quotient rule, we can write

$$\frac{\mathbf{u}_0}{(\gamma - 1)\rho_0^2} \cdot (\rho_0 \nabla p_0 - p_0 \nabla \rho_0) + \frac{p_0}{\rho_0} \nabla \cdot \mathbf{u}_0 = 0.$$

Now we multiply with $(\gamma - 1)$ and use the formula for the sound speed in case of an ideal gas law $c = \sqrt{\frac{\gamma p}{\rho}}$ and receive

$$\frac{\mathbf{u}_0}{\rho_0} \cdot \nabla p_0 - \frac{\mathbf{u}_0 p_0}{\rho_0^2} \cdot \nabla \rho_0 + c_0^2 \nabla \cdot \mathbf{u}_0 - \frac{p_0}{\rho_0} \nabla \cdot \mathbf{u}_0 = 0.$$

The first term can be replaced due to (4.53)

$$-\mathbf{u}_0 \cdot \nabla \Phi - \frac{\mathbf{u}_0 p_0}{\rho_0^2} \cdot \nabla \rho_0 - \frac{\rho_0 p_0}{\rho_0^2} \nabla \cdot \mathbf{u}_0 + c_0^2 \nabla \cdot \mathbf{u}_0 = 0$$

and then the product rule leads to

$$-\mathbf{u}_0 \cdot \nabla \Phi - \frac{p_0}{\rho_0^2} \nabla \cdot (\rho_0 \mathbf{u}_0) + c_0^2 \nabla \cdot \mathbf{u}_0 = 0.$$

Finally, the second term vanishes because of the first equation of (4.55) and we end up with

$$\nabla \cdot \mathbf{u}_0 = \frac{\mathbf{u}_0 \cdot \nabla \Phi}{c_0^2}.$$

References

- [1] Barsukow, W., Edelmann, P.V.F., Klingenberg, C., Miczek, F., Röpke, F. K.: A Numerical Scheme for the Compressible Low-Mach Number Regime of Ideal Fluid Dynamics. *J. of Sci. Comput.* **72**, 623–646 (2017)
- [2] Barsukow, W., Edelmann, P.V.F., Klingenberg, C., Röpke, F.K.: A low Mach Roe-type solver for the Euler equations allowing for gravity source terms. *ESAIM: Proc. Surv.* **58**, 1–10 (2017)
- [3] Berberich, J.P., Chandrashekar, P., Klingenberg, C.: High order well-balanced finite volume methods for multi-dimensional systems of hyperbolic balance laws. *Comput. Fluids* **219** (2021)
- [4] Berberich, J.P., Käppeli, R., Chandrashekar, P., Klingenberg, C.: High order discretely well-balanced method for arbitrary hydrostatic atmospheres. *Commun. Comput. Phys.* **30**(3), 666–708 (2021)
- [5] Berberich, J.P., Klingenberg, C.: Entropy Stable Numerical Fluxes for Compressible Euler Equations which are Suitable for All Mach Numbers. *Proc. Numhyp 2019, SEMA SIMAI Springer Series* (2020)
- [6] Berthon, C.: Stability of the MUSCL schemes for the Euler equations. *Commun Math Sci.* **3**(2), 133–157 (2005)
- [7] Bouchut, F.: *Nonlinear stability of finite volume methods for hyperbolic conservation laws and well-balanced schemes for sources.* *Frontiers in Mathematics*, Birkhäuser Verlag, Basel (2004)
- [8] Bouchut, F., Chalons, C., Guisset, S.: An entropy satisfying two-speed relaxation system for the barotropic Euler equations. Application to the numerical approximation of low Mach number flows. *Numer. Math.* **145**, 35–76 (2020)
- [9] Bouchut, F., Franck, E., Navoret, L.: A low cost semi-implicit low-Mach relaxation scheme for the full Euler equations. *J. of Sci. Comput.* **83**, 24 (2020)
- [10] Chalons, C., Girardin, M., Kokh, S.: An all-regime Lagrange-Projection like scheme for the gas dynamics equations on unstructured meshes. *Commun. Comput. Phys.* **20**, 188–233 (2016)
- [11] Chandrashekar, P., Klingenberg, C.: A second order well-balanced finite volume scheme for Euler equations with gravity. *SIAM J. of Sci. Comput.* **37**(3), B382–B402 (2015)
- [12] Chertock, A., Cui, S., Kurganov, A., Ozcan, S. N., Tadmor, E.: Well-Balanced Schemes for the Euler Equations with Gravitation: Conservative Formulation Using Global Fluxes. *J. Comput. Phys.* **358**, 36–52 (2018)
- [13] Coquel, F., Perthame, B.: Relaxation of energy and approximate Riemann solvers for general pressure laws in fluid dynamics. *SIAM J. Num. Anal.* **35**(6), 2223–2249 (1998)
- [14] Dechallerie, S.: Checkerboard modes and wave equation. *Proc. of Algorith.*, vol. 2009: 71–80 (2009)

- [15] Dellacherie, S.: Analysis of Godunov type schemes applied to the compressible Euler system at low mach number. *J. Comput. Phys.* **229**(4), 978–1016 (2010)
- [16] Desveaux, V., Zenk, M., Berthon, C., Klingenberg, C.: Well-balanced schemes to capture non-explicit steady states in the Euler equations with gravity. *Int. J. Num. Methods Fluids* **81**(2), 104–127 (2016)
- [17] Ferziger, J., Peric, M.: *Computational Methods for Fluid Dynamics*. 3rd ed., Springer, Berlin (2002)
- [18] Harten, A., Lax, P.D., Van Leer, B.: On upstream differencing and Godunov-type schemes for hyperbolic conservation laws. *SIAM rev.* **25**, 35–61 (1983)
- [19] Ismail, F., Roe, P.L.: Affordable, entropy-consistent Euler flux functions II: Entropy production at shocks. *J. Comput. Phys.* **228**, 5410–5436 (2009)
- [20] Käppeli, R., Mishra, S.: Well-balanced schemes for the Euler equations with gravitation. *J. Comput. Phys.* **259**, 199–219 (2014)
- [21] Käppeli, R., Mishra, S.: A well-balanced finite volume scheme for the Euler equations with gravitation - the exact preservation of hydrostatic equilibrium with arbitrary entropy stratification. *Astron. Astrophys.* **587**(A94) (2016)
- [22] Klein, R.: Semi-implicit extension of a Godunov-type scheme based on low mach number asymptotics I: one-dimensional flow. *J. Comput. Phys.* **121**, 213–237 (1995)
- [23] Li, X.s., Gu, C.w.: Mechanism of Roe-type schemes for all-speed flows and its application. *Comput. Fluids* **86**, 56–70 (2013)
- [24] Miczek, F., Röpke, F.K., Edelmann, P.V.F.: New numerical solver for flows at various Mach numbers. *Astron. Astrophys.* **576**(A50) (2015)
- [25] Oßwald, K., Siegmund, A., Birken, P., Hannemann, V., Meister, A.: L2Roe: a low dissipation version of Roe’s approximate Riemann solver for low Mach numbers. *Int. J. Numer. Methods Fluids* **81**(2), 71–86 (2015)
- [26] Rieper, F.: A low-Mach number fix for Roe’s approximate Riemann solver. *J. Comput. Phys.* **230**(13), 5263–5287 (2011)
- [27] Shu, C.-W., Osher, S.: Efficient implementation of essentially non-oscillatory shock-capturing schemes. *J. Comput. Phys.* **77**, 439–471 (1988)
- [28] Suliciu, I.: On modelling phase transitions by means of rate-type constitutive equations. Shock wave structure. *Int. J. Eng. Sci.* **28**(8), 829–841 (1990)
- [29] Thomann, A., Zenk, M., Klingenberg, C.: A second-order positivity-preserving well-balanced finite volume scheme for Euler equations with gravity for arbitrary hydrostatic equilibria. *Int. J. Numer. Methods Fluids* **89**(11), 465–482 (2018)
- [30] Thomann, A., Puppo, G., Klingenberg, C.: An all speed second order well-balanced IMEX relaxation scheme for the Euler equations with gravity. *J. Comput. Phys.* **420** (2020)

- [31] Thomann, A., Zenk, M., Puppo, G., Klingenberg, C.: An all speed second order IMEX relaxation scheme for the Euler equations. *Commun. Comput. Phys.* **28**(2), 591–620 (2020)
- [32] Turkel, E.: Preconditioning techniques in computational fluid dynamics. *Ann. Rev. Fluid Mech.* **31**, 385–416 (1999)
- [33] Xing, Y., Shu, C.-W.: High order well-balanced WENO scheme for the gas dynamics equations under gravitational fields. *J. of Sci. Comput.* **54**, 645–662 (2013)